Traps for Rare Isotopes

Georg Bollen

National Superconducting Cyclotron Laboratory and Department for Physics and Astronomy, Michigan State University, East Lansing, MI, 48824, USA
bollen@nscl.msu.edu

Abstract. Ion traps are widely used in fundamental and applied research. Over the past decade they have also gained significance as tools in experimental nuclear physics. They are used for precision mass measurements, which are important for a better understanding of nuclear structure and the nuclear synthesis of the elements, as well as for precise tests of fundamental interactions. They offer the possibility of textbook-like decay studies, where the nucleus decays in free space. Furthermore, stored ions can be cooled and manipulated in many ways. This is the key to improving the quality of rare isotope beams and for tailoring the beam properties to the needs of the experiments.

1 Introduction

Ion traps are widely used in fundamental and applied research [1–3], but during the past decade they have gained significance as tools in experimental nuclear physics. A main feature is their ability to confine ions in small volumes in well controlled fields. This is the key to precision experiments like mass measurements. Single ions can be stored and detected which makes ion traps highly sensitive devices. Both atom and ion traps offer the possibility of textbook-like decay studies, where the nucleus decays in free space. Furthermore, stored ions can be cooled and manipulated in many ways. This is the key for improving the quality of rare isotope beams and for tailoring the beam properties to the need of the experiments.

Before entering the field of nuclear physics ion traps had already been employed for many purposes. There is a number of types of ion traps, but the two most important ones are Penning traps and Paul, or radiofrequency, traps. Paul traps are mostly used as storage devices for ions which are then studied via laser or radiofrequency spectroscopy or a combination of both [4]. In fact, the first studies related to nuclear physics were the investigation of the hyperfine structure of mostly stable nuclei [5]. Outside of nuclear physics radiofrequency traps are used for trapping small numbers of laser cooled ions for the realization of frequency standards, for the study of coulomb crystals and for quantum computing. They are also used as mass spectrometers, mostly for chemistry and forensic purposes.

Penning traps have become famous for their high precision in a number of measurements. The first measurement was the determination of the electron g-factor by Dehmelt with a precision of $4 \cdot 10^{-12}$ [6]. This result, together with

G. Bollen, Traps for Rare Isotopes, Lect. Notes Phys. **651**, 169–210 (2004)
http://www.springerlink.com/

theoretical calculations [7], serves today to define the fine structure constant. New experiments along this line investigate the g-factor of bound electrons in highly charged ions as a very sensitive test of QED [8]. Other key experiments are the determination of the mass ratios of electron and positron [9,10] and proton and antiproton [11]. The latter has a precision of better than 10^{-10} and provides the most precise hadronic test of the CPT theorem. At Boston a precision of better than 10^{-10} has been achieved in the mass determination of stable isotopes [12]. At Stockholm a Penning trap system is used for the mass measurements of highly charged ions. An example measurement from both places is the mass determination of ^{133}Cs [13,14] which, if combined with photon recoil experiments, is an alternative approach to the determination of the fine structure constant without the need of theoretical input from QED.

The main application for ion traps in nuclear physics that have been developed over the past decade are

- The determination of nuclear binding energies far from stability with Penning trap mass spectrometers.
- The conditioning of rare isotope beams. This includes accumulation, cooling, bunching, and beam purification. Both Penning and Paul traps or related devices are used for these purposes.
- Decay studies of trapped ions for the investigation of correlations in nuclear decays. Again both Penning and Paul traps are employed.

This review will summarize the basic features of ion traps and the experimental techniques used in their connection with rare isotopes. The next chapter will discuss specific differences of ion trap experiments with rare isotopes as compared to stable isotopes. The basic principles of ion trapping and techniques important for the usage of ion traps with rare isotopes will then be presented. Finally, the application of traps will be discussed and examples of ongoing and new projects will be given.

2 Challenges in the Application of Traps to Rare Isotopes

Experiments with short-lived isotopes face specific challenges as compared to those with stable isotopes. For stable (or very long-lived) nuclides a high efficiency in ion production and ion capture is normally not important and a fast measurement technique is not required. The situation is different for most experiments with rare isotopes where two difficulties have to be met in the case of ion trapping:

- The ions are delivered from external sources. Depending on the production schemes the total beam energy can range from several tens of keV to several GeV. The most exotic (and most interesting) species are only created in minute quantities and only a few ions per second or less may

be available. As a consequence, highly efficient schemes for slowing down the fast beams are required. Beam cooling and bunching is mandatory in order to trap ions and store them at low temperatures.
- The farther one recedes from the valley of beta stability, the shorter the half-life of the nuclide to be investigated typically becomes. Half-lives very close to the neutron and proton drip lines range from milliseconds to a few tens of milliseconds. This means that very fast techniques for beam handling, cooling and trapping are required as well as fast measurement techniques, such as the determination of the cyclotron frequency of the stored ions.

Important parameters for trap experiments with rare isotopes are the properties of the rare isotope beam. These properties are mostly determined by the production scheme. In the case of the ISOL (Isotope Separation On-Line) approach, normally a thick target of appropriate material and geometry is bombarded with energetic light ions and rare nuclides are produced by various nuclear reactions. These products diffuse out of the targets, which are kept at high temperature, and eventually reach an ion source. They are ionized, accelerated to an energy of several tens of keV, mass separated in a magnetic sector field and then delivered to the experiments. Examples for such facilities are ISOLDE at CERN [15] and ISAC at TRIUMF [16] in Vancouver. A variation of the ISOL approach are IGISOL systems [17,18] where heavy ions impinge on thin targets. Recoiling reaction products are stopped in a small gas cell, re-ionized by laser light if required, and extracted as low-energy ions that can then be mass separated. A different approach is based on in-flight separation of high energy reaction products. Primary, medium to heavy ion beams are accelerated to energies ranging from MeV/u to GeV/u, depending on the facility and the desired reaction products. These primary ions hit thin targets where new nuclides are produced. The reaction products have a large forward momentum, which makes it possible to mass analyze and select them in flight in magnetic separators. Examples of such facilities are the National Superconducting Cyclotron Laboratory (NSCL) at MSU and the Gesellschaft für Schwerionenforschung (GSI) in Darmstadt.

A major challenge in all production scenarios is the apparent mismatch between the beam properties (i.e. high energy, large emittance) and the requirements of trap-type experiments (i.e. cold ions confined in small volumes). ISOL beams are certainly the easiest to handle due to their low beam energies of a few 10 keV and their good beam quality. This is why ISOLTRAP, the pioneering experiment in this field, is installed at such a facility. Yet, new projects have started to perform measurements on rare isotopes produced by in-flight separation.

The basic principles adopted by all projects for the preparation of the rare isotope beams for their capture in ion traps is illustrated in Fig. 1. In the case of ISOL beams the ions are decelerated electrostatically to low energy before they enter a gas-filled (linear) radiofrequency ion trap. Here the ions

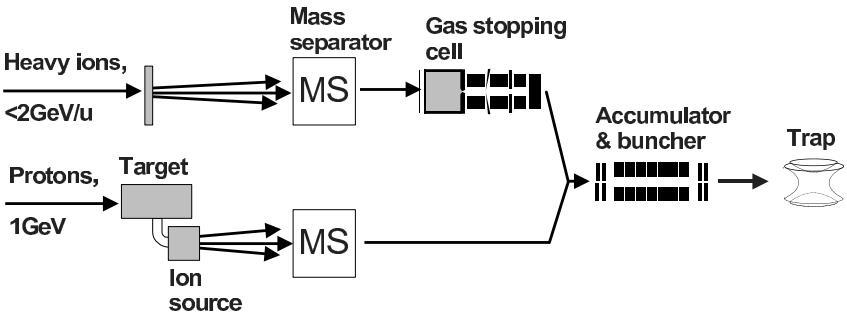

Fig. 1. Beam preparation for precision experiments with trapped ions in the cases of rare isotope production via in-flight separation (top) and the ISOL approach (bottom).

are accumulated and cooled, and finally released as short, cooled ion bunches. In the case of high-energy in-flight separated beams electrostatic deceleration is not practical. Instead, a deceleration procedure is employed which is based on the usage of solid degraders and a stopping cell filled with helium at a pressure ranging from 0.1 to 1 bar. Different schemes are presently being investigated for guiding the ions towards the exit nozzle of the stopping cell, and for their final extraction.

3 Basics of Ion Traps

Two basic methods for trapping charged particles are employed which correspond to the two different types of traps. They are called Penning trap and Paul trap and both are used in nuclear physics.

In the case of the Paul, or radiofrequency quadrupole (RFQ) ion trap, an inhomogeneous radiofrequency field is employed for the ion confinement. This type of traps is well suited for ion accumulation and storage as well as ion cooling and bunching.

The confinement of ions in a Penning trap is achieved by the force due to combined magnetic and electric fields. The presence of the magnetic field allows Penning traps to be employed as mass spectrometers, which is their most important use today.

3.1 Generation of the Electric Trapping Potential

Considering only one dimension z, the parabola is the lowest order polynomial function that describes an electric potential, $V \propto z^2$, in which an ion can be stored. In the case of three dimensions and, demanding cylindrical symmetry, it follows from the Laplace equation that the potential must have a form $V \propto z^2 - \rho^2/2$, where ρ is the distance from the z-axis. This is a quadrupole

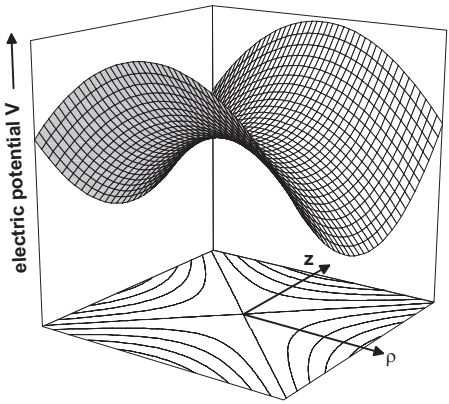

Fig. 2. Quadrupole potential V as a function of the cylinder coordinates ρ and z. The projection shows the equipotential lines.

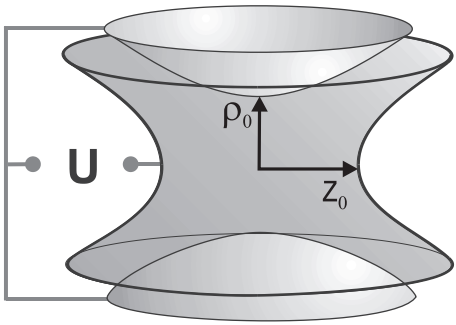

Fig. 3. Basic electrode configuration for the generation of an axially symmetric quadrupole potential. The inner surfaces of the electrodes are hyperboloids and follow equipotential surfaces of the electric field.

as illustrated in Fig. 2. From the figures it becomes clear that a static electric quadrupole potential provides ion confinement only in the axial or the radial direction, depending on the polarity and the ion's charge. Ion confinement in all three dimension requires additional means, which will be discussed in subsequent chapters.

A straightforward way of creating an axially symmetric quadrupole potential is to use a set of electrodes with shapes that follow the equipotential surfaces. Such an electrode system is shown in Fig. 3. This classical configuration for both Penning and Paul traps consists of three electrodes, two so-called endcaps and a ring electrode. The minimum distance between the two endcaps is $2z_0$ and the minimum inner radius of the ring electrode is ρ_0. The electrodes are hyperboloids of revolution and follow the equations

$$z = \sqrt{\rho^2/2 - \rho_0^2/2}, \rho \geq \rho_0 \tag{1}$$

for the ring electrode and

$$z = \pm\sqrt{z_0^2 + \rho^2/2} \tag{2}$$

for the two endcaps.

If a voltage difference U is applied between the endcaps and the ring electrode as indicated in the figure, this system generates the desired quadrupole potential

$$V(\rho, z) = \frac{U}{2d^2} \cdot (\rho^2/2 - z^2) \quad , \tag{3}$$

where $d = \sqrt{\rho_0^2/4 + z_0^2/2}$ is very useful measure of the characteristic trap dimension.

The configuration shown in Fig. 3 is not perfect as it does not generate a pure quadrupole potential. The reason is that the electrodes do not extend to infinity. The result of such a truncation can be higher-order multipole components in the trapping potential. Other sources for higher-order multipoles are imperfect electrode shapes or holes in the endcaps which are required to the injection and ejection of the ions. If ion storage is the only concern then this is not a problem. But for precision Penning trap mass spectrometry, systematic frequency shifts can occur which reduce the accuracy of the measurement. Therefore, additional correction electrodes are normally employed for the compensation of higher-order multipoles and in order to minimize their effects.

Figure 4 shows two axial-symmetric ion trap configurations that are presently used in the ISOLTRAP experiment at CERN. The left configuration is a high precision trap for mass measurements. It is equipped with two pairs of correction electrodes. The other is a cylindrical trap which is used for rare isotope beam purification, ion cooling and bunching (see below). In its central region an approximated quadrupole potential is achieved by applying appropriate voltages to the cylindrical electrodes.

The classical configuration for radiofrequency ion traps is the one shown in Fig. 3 but there exist quite different configurations that are also widely used. Some of them will be briefly presented in the following chapter.

3.2 Ion Confinement in Paul or RFQ Traps

In the case of Paul or RFQ traps ion confinement is obtained by oscillating electric fields. How is this possible with a saddle-shaped potential as shown in Fig. 2? If we assume this potential to be static then an ion is confined in one direction but will slide down the potential surface in the other direction. An intuitive counteraction would be to quickly change the polarity of the potential and to force the ion to slide back, with the result that the ion might now escape in the other direction, demanding for another counteraction and

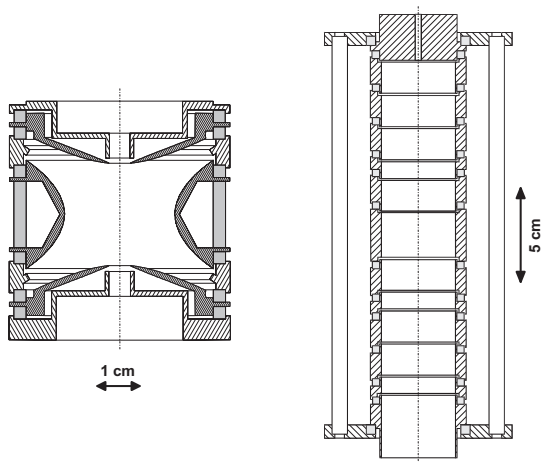

Fig. 4. Electrode configurations for Penning traps as used in the ISOLTRAP experiment at CERN. Left: highly-compensated hyperbolic trap. Right: Cylindrical trap.

so forth. This leads indeed to ion confinement and we follow a discussion presented earlier by Dehmelt [19].

In order to illustrate the origin of the confining force, Fig. 5 compares the cases of an ion with charge e in an homogeneous and an inhomogeneous electric field. In the homogeneous field the ion experiences a position independent force that changes direction and magnitude periodically due to the applied rf voltage. Averaged over time the net force acting on the ion is zero. The ion oscillates forth and back but its average position does not change. This is different in the case of an inhomogeneous electric field. Here the oscillation of the ion in the rf-field (micro motion) gives rise to a non-zero net force F_n that slowly drives the ion (macro motion) towards a region of weaker electric rf-field strength.

In the case of RFQ traps a voltage $U(t) = U_{\mathrm{DC}} + U_{\mathrm{rf}} \cdot \sin(\omega_{rf} \cdot t)$ is applied to the electrode configuration as shown in Fig. 3. This creates an oscillating quadrupole potential. The magnitudes of the electric field strength in both the axial and radial direction, $|E_\rho| \propto \rho$ and $|E_z| \propto z$ increase linearly with the distance from the trap center. The same is true for the magnitude of the instantaneous force eE acting on the ions and also the time-averaged force $\vec{F_n} \propto -\vec{r}$. The ion will therefore perform a bound, harmonic (macro) motion about the trap center. Figure 6 shows such ion trajectories in a Paul trap for two different parameter sets. The projections clearly depict the superposition of harmonic macro and micro motion.

The force $\vec{F_n} = -e\vec{\nabla}V_{pseudo}$ can be regarded to result from a static pseudo potential $V_{pseudo}(\rho, z)$ that has the form of a parabolic well. Following the arguments given above this pseudo potential can be derived analytically [19]

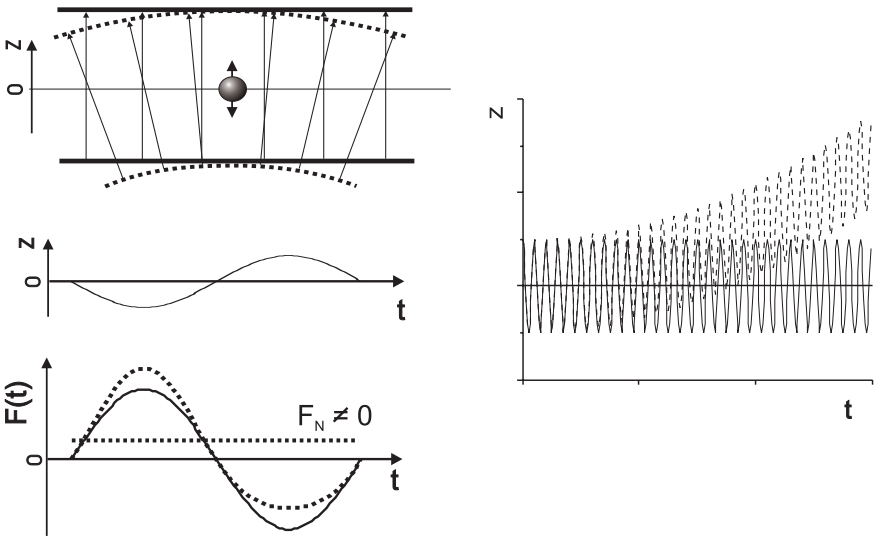

Fig. 5. Illustration of the origin of the effective force F_n in an inhomogeneous electric field. Top: ion placed between to parallel plates and two bent plates between which an oscillating voltage is applied. Middle: One oscillation of ion about its local position. Bottom: Force acting on the ion as a function of time for the parallel plates (solid line) and the bend plates (dashed line) Right: long term effect of the oscillating field on the ion's position in both cases.

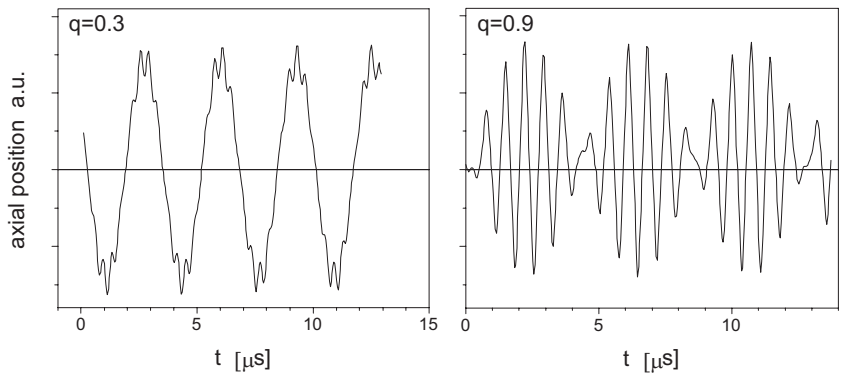

Fig. 6. Motion of an ion in an RFQ trap for two different rf amplitudes corresponding to Mathieu parameters $q = 0.3$ and $q = 0.9$.

and is described by

$$V_{\text{pseudo}}(\rho, z) = \frac{e}{m}\left(\frac{U_r}{2\omega_{rf} d_0^2}\right)^2 (\rho^2/4 + z^2). \tag{4}$$

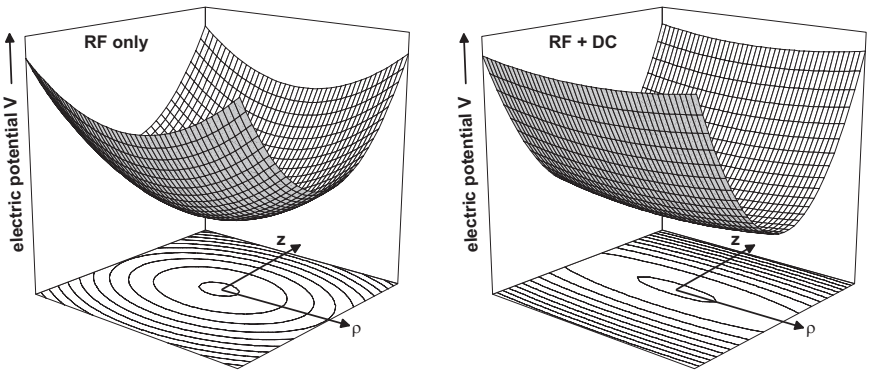

Fig. 7. Pseudopotential in a Paul trap. Left: only rf potential applied to the trap. Right: with additional DC-potential.

An ion performs harmonic motions in this parabolic potential (Fig. 7) with frequencies[1]

$$\omega_z = \frac{e}{m}\frac{U_{rf}}{\sqrt{2}\omega_{rf}d^2} \tag{5}$$

in the axial and

$$\omega_\rho = \frac{1}{2}\omega_z \tag{6}$$

in the radial direction.

As an example we consider a trap with parameters as given in Table 1. In this trap a singly charged ion with mass number $A = 50$ experiences a trapping potential well of 11.0 V depth along the z-axis and 5.5 V depth in radial direction. This results in frequencies for the macro motions of 104 kHz and 52 kHz.

If a DC voltage U_{DC} is applied in addition to the rf voltage, the resulting effective potential can in first order be obtained by simply adding the resulting DC potential (3) and the pseudo potential (4), $V_{DC+rf} = V(\rho, z) + V_{pseudo}(\rho, z)$. For a given polarity of the DC voltage the depth of the total potential well will increase in one direction and decrease in the other, as illustrated in Fig. 7 (right). The figure makes clear that beyond a certain DC voltage ion confinement in all dimensions will no longer be obtained.

Also in the rf-only case the ion motion is only stable for a limited parameter range. The arguments given above for the origin of the effective force F_n will no longer hold if if we increase the rf amplitude to a point where the

[1] The reader should be warned that the term frequency will be loosely applied to both the angular velocity ω and the actual frequency $\nu = \omega/2\pi$. ω will be used mostly in the context of theoretical discussions while ν will be used in number examples.

Table 1. Example of parameters for a Paul and a Penning trap. These parameters are typical and will be used throughout this article.

Trapping electrodes	
Inner radius of ring electrode ρ_0	1.4 cm
Distance between endcaps $2z_0$	2.0 cm
Characteristic trap dimension d	1.0 cm
Paul trap	
rf amplitude U_{rf}	300 V
rf frequency ν_{rf}	1 MHz
DC-voltage U_{DC}	0 V
Penning trap	
Magnetic field strength B	9.4 T
Trapping voltage U	10 V

macro frequency comes close to the rf frequency. In order to examine this further it is instructive to consider an analog system.

The storage of ions by oscillating electric fields is equivalent to the focussing of charged particle or light beams in alternating gradient transport systems, where focussing and defocussing optical elements alternate in space. Such systems are very common and can be found in the beam transport systems in accelerators as well as in the beam lines for the delivery of rare isotopes to experiments. In fact, the analogy to ion traps is employed to learn more about the physics of beam transport systems [20,21]. The reason for this being possible is that in the rest frame of the moving ion there is no difference to being confined by an oscillating inhomogeneous electric field. For the purpose of illustration we will use a light optical system instead of an ion optical system. Figure 8 shows sets of convex and concave lenses, where in each set the lenses have the same focal length. The top figure shows a situation in which overall focussing is achieved. The second case illustrates the effect of a focussing too weak for a given distance between the optical elements. The last case illustrates a situation in which the focussing (respectively defocussing) strength of the elements is too large for the given geometry. Applying these observations to the case of a Paul trap leads one to conclude that the rf amplitude (focal strength of optical elements) and the rf frequency (distance between optical elements) have to stay within certain limits in order to achieve stable motion and confinement.

In order to evaluate in detail which parameters result in stable ion trajectories it is necessary to solve the equation of motion. For an axially symmetric rf quadrupole potential

$$U(t) = U_{\mathrm{DC}} + U_{\mathrm{rf}} \cdot \cos(\omega_{rf} \cdot t) \tag{7}$$

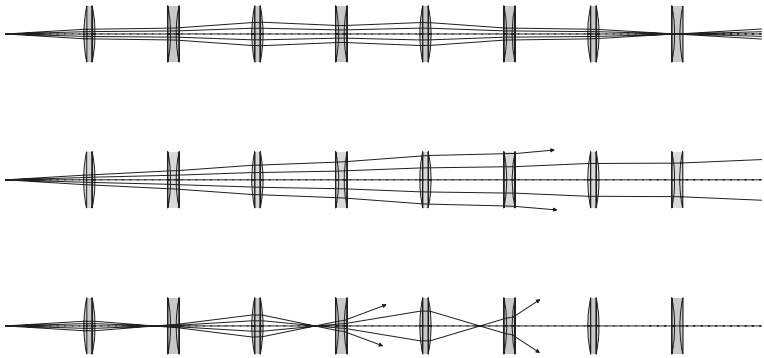

Fig. 8. Focussing-defocussing optical system with alternating convex and concave lenses with the same focal lengths. A different index of refraction has been used for each simulation shown. Top: overall focussing is achieved. Middle: too weak focussing. Bottom: too strong focussing.

the equations for an ion with charge e and mass m are

$$\ddot{\rho} = \frac{e}{m}\frac{\rho}{2d^2} \cdot U(t) \tag{8}$$

$$\ddot{z} = \frac{e}{m}\frac{z}{d^2} \cdot U(t)\,. \tag{9}$$

There is no simple analytic solution for these equations but they can be brought into the form of the so-called Mathieu equation. This differential equation describes a large variety of oscillatory problems and its solution is an infinitive series of harmonic functions. The Mathieu equation has the general form

$$\frac{d^2s}{d\xi^2} + (a - 2q\cos 2\xi) \cdot s = 0\,. \tag{10}$$

In order to use the Mathieu equation the following substitutions have to be made. For the axial motion s is replaced by z and for the radial motion by ρ and the phase $\xi = \omega_{rf}(t/2)$ is used. The Mathieu parameters a and q for the axial and the radial motions are

$$a_z = \frac{4eU_{DC}}{m\omega_{rf}^2 d^2} \tag{11}$$

$$q_z = \frac{2eU_{rf}}{m\omega_{rf}^2 d^2} \tag{12}$$

$$a_r = -\frac{a_z}{2} \tag{13}$$

$$q_r = -\frac{q_z}{2} \tag{14}$$

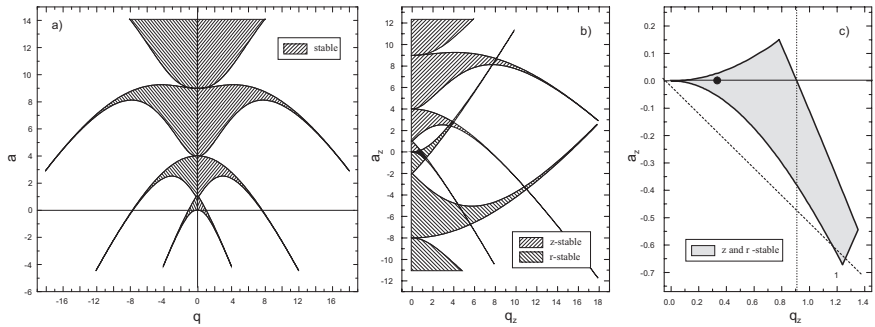

Fig. 9. a) Regions of stable solutions of the Mathieu equation. b) Regions of stable solutions for both the axial and radial motion in a Paul trap. c) Enlarged area of Fig. b). The points indicated correspond to working points discussed in the text. The line indicates a working line for which the Paul trap can be operated as a mass separator.

For our discussion it is sufficient to know which parameters lead to stable solutions. For this purpose we can use the so-called Mathieu diagram (Fig. 9a) which shows the regions of stable solutions in the parameter space for a and q.

With the last two relations between the Mathieu parameters for the axial and radial directions one can construct a combined stability diagram for both the axial and radial direction by superposing those for each direction. The result is shown in Fig. 9b. Ion storage is achieved where the regions of stable motion in the axial and radial direction overlap. The largest stability region is located close to the origin and is shown enlarged in Fig. 9c. The point of operation for the example of the ion with A=50 given above corresponds to $a_z = 0$ and $q_z = 0.3$ and is indicated in the figure. The motion becomes unstable if $q > q_{max} = 0.908$. In our example this may be caused by increasing the rf amplitude from $U_{rf} = 300\,\mathrm{V}$ to 928 V or by decreasing the rf frequency from $\nu_{rf} = 1\,\mathrm{MHz}$ to 569 kHz. Figure 6b shows the ion motion close to this point.

So far we have only considered Paul traps with hyperbolic electrodes. In fact there are many other useful configurations which have in common that either the complete or at least part of the trapping mechanism relies on an ion moving in an oscillating inhomogeneous electric field. The most important are linear quadrupole and also hexapole configurations and stacks of open disks to which alternating voltages are applied. The simple quadrupole and hexapole systems shown in the figure will provide focussing only in the axial direction. One of their main uses for rare isotope beams is as ion guides and as part of ion beam coolers (see below). In order to achieve trapping additional electrodes or segmented rf-electrodes are required which allow generation of an axial confinement potential by applying appropriate voltages. The disk

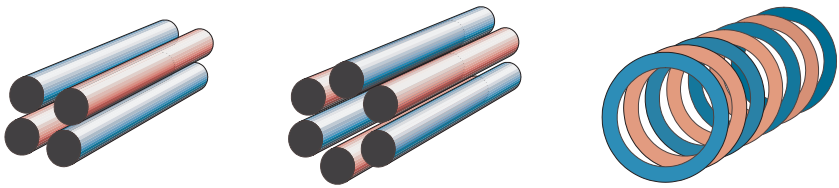

Fig. 10. Other electrode configurations used for radiofrequency ion traps and ion guides.

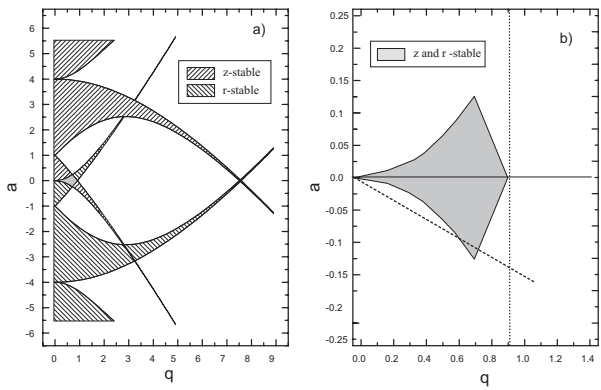

Fig. 11. Regions of stable solutions for a linear radiofrequency quadrupole.

system on the right can in principle be used for ion trapping since additional static voltages can be applied in addition to the rf voltage.

Here, only the linear quadrupole will be considered in more detail. Figure 11 shows its stability diagram. The Mathieu parameters a and q are the same for the x and y direction and given by

$$a = 8\frac{eU_{DC}}{mr_0^2\omega_{rf}^2} \tag{15}$$

$$q = 4\frac{eU_{rf}}{mr_0^2\omega_{rf}^2}\ , \tag{16}$$

where $2r_0$ is the separation between the surface of opposite electrodes. The resulting pseudo potential is given by

$$V_{pseudo}(r) = \frac{q \cdot U_{rf}}{4r_0^2}r^2 = \frac{e}{m}\left(\frac{U_{rf}}{r_0^2\omega_{rf}}\right)^2 r^2 \tag{17}$$

and to a good approximation for $q < 0.4$, its macro oscillation frequency is

$$\omega_{\mathrm{m}} = \frac{q}{\sqrt{8}}\omega_{\mathrm{rf}}\ . \tag{18}$$

As an example, a singly charged ion with mass number $A = 39$ in a 4-rod structure with $r_0 = 10\,\mathrm{mm}$ operated with $\nu_{rf} = 1\,\mathrm{MHz}$, $U_{\mathrm{rf}} = 100\,\mathrm{V}$ will

experience a depth of the radial trapping potential of about 6.3 V in which it oscillates with $\omega_m = 89\,\text{kHz}$.

A feature of all radiofrequency traps and ion guides is their ability to act as mass filters. This feature finds a very common application in rest gas mass analyzers most of which are based on linear radiofrequency quadrupoles. Mass spectrometers based on hyperbolic traps are used for a variety of analytical purposes. As can be seen from (8) both a and q are mass dependent. This means that for given trap parameters there is only a range of masses that can be stored. Taking again the rf-only example given above, we find a lower mass limit of A=17. However, in order to operate a Paul trap or a linear rf trap as a mass filter it is necessary to find operating parameters that allow only ions in a narrow mass range to be stored. This is the case in the upper or lower tips of the stability diagram. Therefore, a DC-voltage is required. A mass scan is usually performed by simultaneously changing both rf and DC voltages along a working line as shown in Figs. 9 and 11. Only ions with a and q values in the range where the line is inside the stability area will perform a stable motion. The closer this line is to the tip of this area the higher is the resolving power of the mass filter.

3.3 Penning Traps

In Penning traps the storage of an ion with mass m and charge q is accomplished by combining a strong magnetic field $\vec{B} = B\hat{z}$ with a static potential V_{DC}, (3) created by a voltage U_{DC} applied to the trap electrodes as shown in Fig. 12.

In order to understand the trapping of ions in a Penning trap let us first consider the case in which no electric field is present as illustrated in Fig. 12 (left). If an ion with mass m and charge q has a velocity component v perpendicular to the direction of the magnetic field $\vec{B} = B\hat{z}$ it will experience

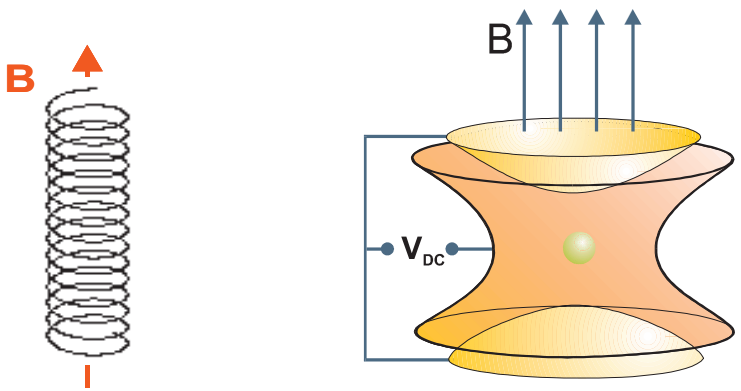

Fig. 12. Penning trap principle. Left: cyclotron motion of an ion in a magnetic field. Right: Basic Penning trap configuration

Table 2. Cyclotron, reduced cyclotron, axial, and magnetron frequencies for ions with mass number A and charge state Q for trap parameters as given in Table 1.

Q	A	ν_c	ν_+	ν_z	ν_-
1	4	36136849	36136003	247355	847
1	50	2890947	2890101	69963	847
1	200	722736	721889	34981	848
1	42686	3386	1697	2394	1689

a Lorentz force $F_L = q \cdot \vec{v} \times \vec{B}$. This force leads to a circular motion with angular frequency

$$\omega_c = \frac{e}{m} \cdot B \quad , \tag{19}$$

and radius $\rho = v/\omega_c$. The cyclotron frequency ν_c for a singly charged ion with mass number 50 is $\nu_c = \omega_c/2\pi = 2.9\,\mathrm{MHz}$ in a 9.4 T field (see Table 2). If the ion has a kinetic energy of 1 eV (corresponding to $v = 2$ km/s) the radius of the circular motion is $r = 0.1\,\mathrm{mm}$.

The cyclotron motion implies that the ion motion is radially bound to a magnetic field line going through its center. However, there is no binding in the direction of the magnetic field lines and if the ion has any velocity component in this direction it will escape as illustrated in the figure. Axial confinement in a Penning trap is achieved by superposing a static electric quadrupole potential as illustrated in the figure. The harmonic potential well in the axial direction provides the necessary restoring force and the equation of motion in the axial direction is

$$m\ddot{z} = -e\frac{U}{d^2}z \quad . \tag{20}$$

This corresponds to a harmonic oscillation with angular frequency

$$\omega_z = \sqrt{\frac{eU}{md^2}} \quad . \tag{21}$$

Table 2 gives the axial frequencies for ions with different masses.

How does the radial de-focussing of the static electric potential affect the radial motion of the ion? To which limit can the strength of the quadrupole potential be increased without loosing the ion? In order to answer these questions we consider an ion moving about the z-axis and in the x-y plane on a circle with radius ρ with speed v. The force F_c that leads to this circular orbit is now the sum of the Lorentz force F_L and the electric force F_E

$$m\ddot{\rho} = F_c = F_L + F_E \tag{22}$$

$$-m\frac{v^2}{\rho} = -e \cdot v \cdot B + e\frac{U}{2d^2}\rho \tag{23}$$

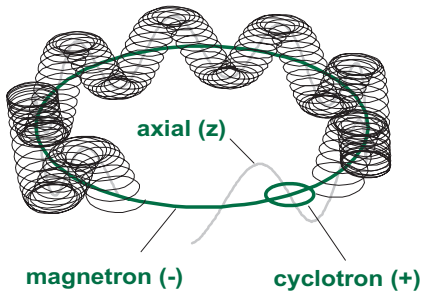

Fig. 13. Schematic of the motion of an ion in a Penning trap

With $v = \omega\rho$, $\omega_c = e/m \cdot B$ and $(e/m)U/(2d^2) = \omega_z^2/2$ this can be written as

$$\omega^2 = e/mB\omega - e/mU/(2d^2) = \omega_c\omega - \omega_z^2/2 \ . \tag{24}$$

This equation has two solutions for ω

$$\omega_\pm = \frac{\omega_c}{2} \pm \sqrt{\frac{\omega_c^2}{4} - \frac{\omega_z^2}{2}} \ . \tag{25}$$

This means that two types of radial motion exist. They are called (reduced) cyclotron motion and magnetron motion. Table 2 gives again the frequencies for ions with different masses. Any superposition of both motions is also a solution of the equation of motion (22). Including the axial motion the position of the ion in the trap can therefore be described by

$$x = \rho_+ \cos(\omega_+ t + \phi_+) + \rho_- \cos(\omega_- t + \phi_-) \tag{26}$$

$$y = \rho_+ \sin(\omega_+ t + \phi_+) + \rho_- \sin(\omega_- t + \phi_-) \tag{27}$$

$$z = \rho_z \cos(\omega_z t + \phi_z) \ , \tag{28}$$

where $\rho_{+,-,z}$ are the amplitudes of the radial and axial motions and $\phi_{+,-,z}$ are the corresponding phases. The motion is depicted schematically in Fig. 13. It shows the superposition of three harmonic motions, the axial oscillation, the magnetron motion and the modified cyclotron motion with eigen frequencies ω_z, ω_-, and ω_+.

By comparing the magnitudes of the eigen frequencies (see Table 2) one finds the following order

$$\omega_+ > \omega_z > \omega_- \ . \tag{29}$$

Other important relations between the eigen frequencies and the cyclotron frequency are

$$\omega_c = \omega_+ + \omega_- \tag{30}$$

and

$$\omega_c^2 = \omega_+^2 + \omega_z^2 + \omega_-^2 \tag{31}$$

$$\omega_z^2 = 2\omega_+\omega_- \ . \tag{32}$$

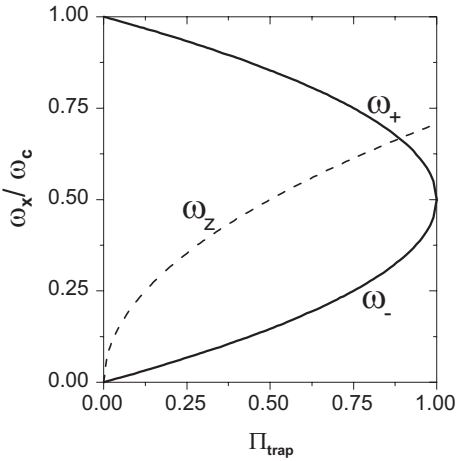

Fig. 14. Ratio of the eigen frequencies of an ion and its cyclotron frequency as a function of the trapping parameter $\Pi_{trap} = 2(\omega_z/\omega_c)^2$. For $\Pi_{trap} > 1$ the radial motion becomes unstable.

Equation 30 is the key to high precision mass measurements since it allows to determine the cyclotron frequency of the ions if the individual frequencies of the radial motion or their sum can be measured. This will be discussed in more detail later.

Under normal operating conditions represented by the first three cases listed in Table 2 we find $\omega_+ >> \omega_-$. It is observed that the magnetron frequency is largely mass independent. Expanding the root for the magnetron frequency to first order indeed yields

$$\omega_- \approx U/(2Bd^2) \ , \tag{33}$$

Throughout the rest of this document and if not stated otherwise we will assume that $\omega_+ >> \omega_-$ and several formulas will be simplified using this assumption.

The next question to be addressed is the stability of the ion motion. The frequencies in (21) and (25) have to be real to obtain a stable motion. For the axial motion this means that $q \cdot U > 0$.

For the radial motion we can introduce a parameter [22]

$$\Pi_{trap} = 2(\omega_z/\omega_c)^2 = \frac{m}{q}\frac{2U}{d^2B^2} \ , \tag{34}$$

which can be regarded as a measure of the relative strength of electric and magnetic field. Stable radial motion is achieved if $\Pi_{trap} < 1$. For $\Pi_{trap} = 1$ magnetron and reduced cyclotron frequency are equal to $\omega_c/2$. Figure 14 shows the eigen frequencies of an ion relative to its cyclotron frequency ω_c as a function of the stability parameter Π_{trap}.

As can be seen from (34), for given trap parameters U, B, and d an upper mass-over-charge ratio limit exists for the ion to be stored. For trap parameters as given in Table 1 singly-charged ions with a maximum mass number of A=42686 could be stored (see Table 2).

In order to understand some of the features of the ion motion in a Penning trap it is useful to consider the energy of the motion. The total energy of an ion moving in a Penning trap is the sum of the potential and kinetic energies of each eigen motion,

$$E = E_z + E_+ + E_- = \frac{m}{2}\rho_z^2\omega_z^2 + \frac{m}{2}\rho_+^2(\omega_+^2 - \omega_+\omega_-) + \frac{m}{2}\rho_-^2(\omega_-^2 - \omega_+\omega_-) \quad . \tag{35}$$

The potential energies $-e(U/d^2)\rho_\pm^2 = -m\rho_\pm^2\omega_z^2 = -\frac{m}{2}\rho_\pm^2(\omega_+\omega_-)$ of the radial motions are negative, reflecting the fact that the ions experience a potential hill in the radial direction. Since $\omega_+ > \omega_-$, the total energy of the reduced cyclotron motion is positive while that of the magnetron motion is always negative. This has important consequences in the case of an energy loss of the ion motion, for example due to collisions with residual gas or a buffer gas present in the trap. The axial and cyclotron motion behave normal in the sense that any energy loss reduces their amplitudes. In contrast to this, the amplitude of the magnetron motion increases and if no further counteractions are taken the ion may finally be lost. In Chap. 3.6 this issue is discussed in more detail.

3.4 Ion Motion Excitation in Penning Traps

The resonant excitation of the ion motion is of importance for the determination of the frequencies of the ion motion for mass measurements, the selective removal of ions from the trap, or for counteracting the effect of ion loss via a growing magnetron motion discussed above. The ion motion in a Penning trap can be driven very selectively by applying radiofrequency fields. The result of the excitation depends on the applied frequency and the multipolarity of the rf field.

Dipole excitation. A dipole rf field in either the axial or any radial direction can be used to change the amplitude of the axial oscillation or of one of the radial motions independently. An axial dipole field generated by applying an rf voltage between both endcaps drives the axial motion if the rf frequency is equal to ν_z. A dipole field created by an rf voltage applied between two opposite segments of the ring electrode drives one of the radial motions if the corresponding frequency is used. Each eigen motion behaves like a simple driven harmonic oscillator. In resonance, the amplitude of an eigen motion will eventually grow linearly, but the initial behavior depends on the initial position and velocity of the ion and the phase of the rf field.

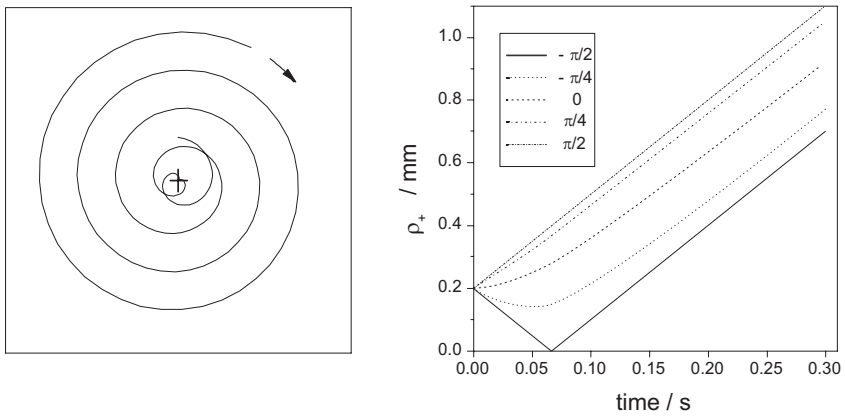

Fig. 15. Radial motion of an ion in the case of dipole excitation of the cyclotron motion. Left: Ion trajectory in the x-y plane. Right: Change of amplitude ρ_+ as a function of time for different initial relative phases $\phi_+ - \phi_{rf}$. The solid curve corresponds to the trajectory shown on the left.

This is illustrated in Fig. 15 in the case of an excitation of the cyclotron motion with an initial amplitude and a particular phase difference between rf field and motion chosen.

Dipole excitation of the ion motion is normally used to drive the ion to a specific orbit but also to remove ions from the trap. Mass selectivity is achieved by driving the axial or cyclotron motion of one ion species. If it is desired to drive all ions to larger orbits simultaneously then the magnetron frequency can be used since it is practically mass independent. For this case the change of amplitude with time t is approximately given by

$$\rho(T_{rf}) \approx \frac{V_{rf}}{2aB} T_{rf} \ , \tag{36}$$

where a is approximately equal to the inner radius ρ_0 of the ring electrode. The same equation holds also for the reduced cyclotron motion. The response of the ion motion to the rf field as discussed so far takes of course only place if ν_{rf} equals one of the eigenfrequencies and if the field orientation is correct. For other frequencies the ion motion will go out of phase with the driving field and the maximum amplitude will be limited. The change of amplitude as a function of the detuning $\Delta\omega = 2\pi\Delta\nu = \omega_{rf} - \omega_x$ of the rf-frequency from one of the eigen frequencies ω_x gives a resonance profile, which follows a $\frac{\sin^2(\Delta\omega)}{\Delta\omega^2}$ law, as shown in Fig. 16.

Quadrupole excitation. The quadrupole is the other important multipolarity used for the manipulation of the ion motion. Quadrupolar rf fields allow the ion motion to be excited at differences or sums of the eigen frequencies, as for example $2\omega_z$, $\omega_+ - \omega_z$, or $\omega_+ + \omega_-$. This type of excitation is often

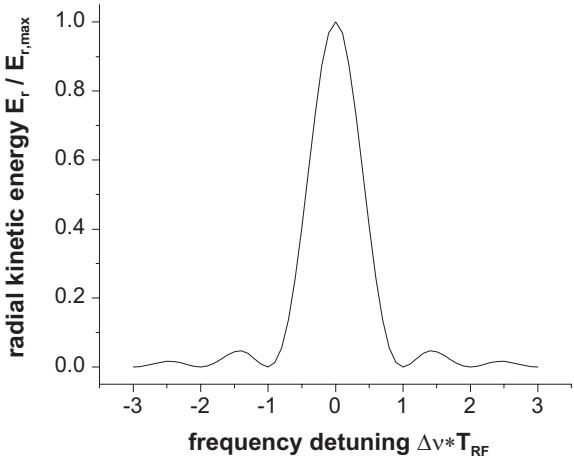

Fig. 16. Radial energy of the ion motion in the case of dipole excitation near ν_+ as a function of the detuning $\Delta\nu = \nu_{rf} - \nu_+$. The energy is normalized to the maximum and the detuning to the reciprocal of the excitation time T_{rf}.

called side-band excitation. Not only the frequency but also the orientation of the quadrupole determines if the ion motion responds resonantly to the excitation or not. In fact, each of the examples just listed requires a different orientation. The most important case with respect to its application to rare isotopes is the quadrupole excitation at the sum $\omega_+ + \omega_-$ of the frequencies of magnetron and cyclotron motion. For this case an azimuthal quadrupole is required which can be realized by dividing the ring electrode into four segments.

The excitation at $\omega_+ + \omega_-$ is important with regard to mass measurements since this sum frequency equals the cyclotron frequency $\omega_c = e/m \cdot B$. Later we will see (Chap. 3.6) that it is also important in connection with buffer gas cooling in Penning traps.

The details of azimuthal quadrupole excitation of ion motion have been discussed in [23,24]. Only the main features will be presented here. The most important one is that this type of excitation couples both radial motions. The coupling is very similar to that of an atomic two-level system where a Rabi oscillation occurs between both levels caused by resonant excitation. Figure 17 shows the effect of quadrupole excitation at ν_c. Initially there is only magnetron motion. As a consequence of the excitation the amplitude of the magnetron motion decreases while the amplitude of the cyclotron motion increases. After some period of time the magnetron motion has disappeared and the amplitude of the cyclotron motion is that of the initial magnetron motion. Now the change of amplitudes is reversed. The overall effect is a harmonic beating between magnetron and cyclotron motion as depicted in Fig. 18. For $\omega_{rf} = \omega_c$ the beating frequency Ω_0 is proportional to the ampli-

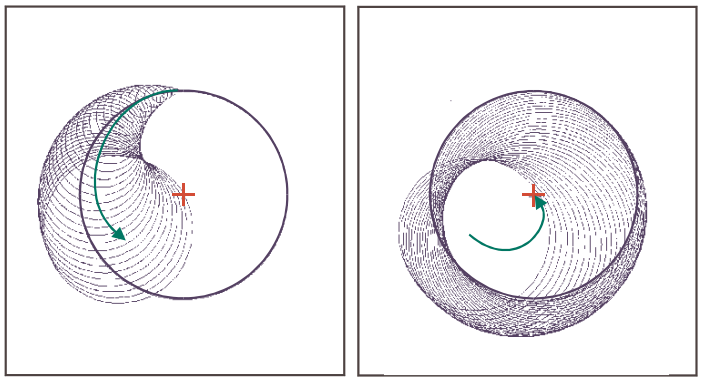

Fig. 17. Radial motion in the case of quadrupole excitation at $\nu_{rf} = \nu_c$. The motion starts with pure magnetron motion, indicated by the circle.

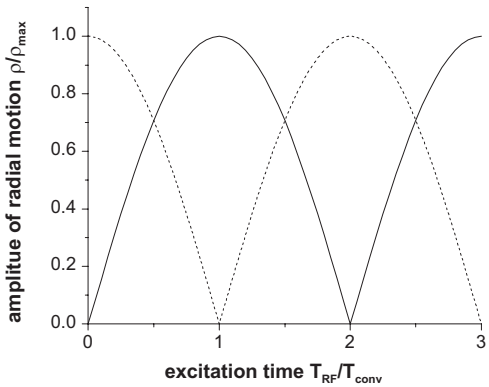

Fig. 18. Magnetron (dashed line) and cyclotron amplitude (solid line) as a function of the ratio T_{rf}/T_{conv} of excitation time to conversion time.

tude V_{rf} of the rf field. For $\omega_+ \gg \omega_-$ it is

$$\Omega_0 = \frac{V_{rf}}{a^2}\frac{1}{4B} \tag{37}$$

V_{rf} corresponds to the maximum potential of the quadrupole rf field measured on a circle with radius a. The beating frequency is practically mass independent.

A conversion from a pure magnetron to a pure cyclotron motion is obtained after a time T_{conv} which is half the beating period

$$T_{conv} = \frac{\pi}{\Omega_0} = \frac{4\pi a^2 B}{V_{rf}} \tag{38}$$

As an example we consider an ion in a 9 T field. In good approximation we can assume that a is equal to the inner radius of the ring electrode, which is

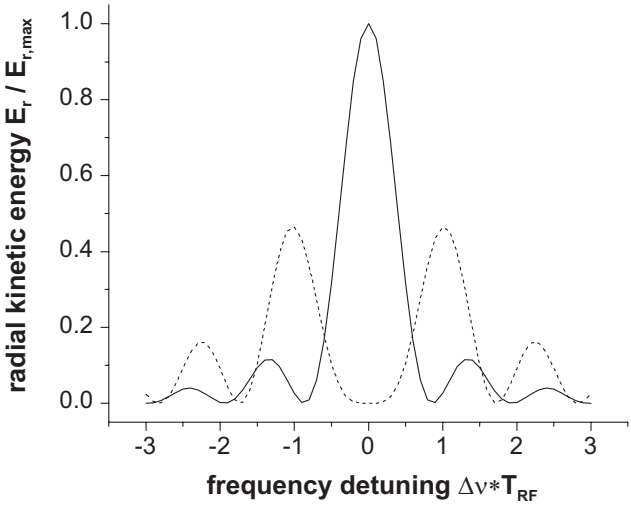

Fig. 19. Radial energy of the ion motion in the case of quadrupole excitation near ν_c as a function of the detuning $\Delta\nu = \nu_{rf} - \nu_c$. The energy is normalized to the maximum and the detuning to the reciprocal of the excitation time T_{rf}. The solid curve corresponds to $T_{rf} = T_{conv}$ and the dashed curve to $T_{rf} = 2 \cdot T_{conv}$

typically 1 cm. Application of an rf amplitude of $V_{rf} = 10\,\mathrm{mV}$ results in a conversion time T_{conv} of about one second.

If the initial condition is not a pure magnetron or cyclotron motion then the beating will normally not be complete and the minimum and maximum amplitude will depend on the initial amplitudes, as well as on all phases involved. In practise, one therefore tries to realize a situation close to the ideal case shown in the figures.

The response of the ion motion to the rf field as discussed above takes only place if $\omega_{rf} = \omega_c$. For other frequencies the conversion from one motion into the other will not be completed. This is reflected in the resonance profiles for the amplitudes shown in Fig. 19. Again the radial energy is shown as a function of the detuning. In contrast to the dipole case the shape of the profile depends on the product $T_{rf} \cdot A_{rf}$. If this pair of parameters is chosen such that an initially pure magnetron motion is converted into a pure cyclotron motion or vice versa, then a profile is obtained as shown by the solid line. A profile as shown by the dashed line is observed for an amplitude for which a full beat period is completed at the end of the excitation. Here the initial magnetron motion has been re-established which results in minimum radial energy. The energy gain as a function of the detuning $\Delta\omega = \omega_{rf} - \omega_c$ is described by

$$E_r(\Delta\omega) = \frac{e^2 V_{rf}}{32 m a^4} \frac{\sin^2(\Omega T_{rf})}{\Omega^2} \tag{39}$$

with the beating frequency

$$\Omega = \Omega(\Delta\omega) = \frac{1}{2}\sqrt{\Delta\omega^2 + 4\Omega_0^2} \tag{40}$$

From a measurement of such profiles the cyclotron frequency of the ion can be determined as will now be discussed.

3.5 Frequency Measurements in Penning Traps

A number of techniques have been developed for the determination of the eigen frequencies, or combinations of them. In many experiments techniques are used which are based on the detection of image currents induced in the trap electrodes. These signals can for example be Fourier analyzed and in this way the motional frequencies be determined. This technique, called Fourier-transform Ion Cyclotron (FT-ICR) mass spectrometry is widely applied in analytical chemistry and works very well if many ions are stored. Another possibility is to employ tuned circuits, which can reach single-ion sensitivity. This technique has been employed in a number of high precision experiments on stable ions and charged elementary particles, where preparation time plays a minor role. Its applicability is also under investigation for the study of superheavy elements which are rather long-lived but have extremely low production rates.

For the investigation of short-lived isotopes a quite different technique has established itself to be the best choice. It is based on time-of-flight detection [25] of the change of the cyclotron energy $E_c(\omega_{rf}) \approx E_+(\omega_{rf}) = m/2\omega_+^2\rho_+^2(\omega_{rf})$ of the ion motion resulting from a preceding excitation with frequency ω_{rf}. The magnetic moment $\vec{\mu}(\omega_{rf}) = [E_c(\omega_{rf})/B]\hat{z}$ of the ion's orbit is proportional to the energy of the cyclotron motion and is conserved if the magnetic field strength B is slowly changed. If an ion is allowed to drift along the axis $\hat{z}$ of the solenoid which provides the magnetic field it will eventually enter a region where the magnetic field strength decreases. Here, the ion experiences an accelerating force $\vec{F} = -\vec{\mu}(\omega_{rf})(\partial/\partial z\, B(z))$ which is proportional to its orbital magnetic moment and to the gradient of the magnetic field. This is used for the detection of resonances in the change of the radial energy as illustrated in Fig. 20. After the capture of the ion the motion is excited with a trial frequency ν_{rf} close to the expected cyclotron frequency for a fixed excitation time T_{rf}. The ion is then ejected from the trap by switching the trap potentials appropriately. It drifts out of the strong homogenous part of the magnetic field and passes through the region of decreasing field strength. Here the ion experiences the accelerating force F which will be largest if the ion has gained maximum radial energy due to the rf excitation. Finally, it hits an ion detector located in the weak fringe field. Its time of flight T from the trap to the detector is measured and will be shorter for a larger gain in radial energy. The trap is reloaded and a new trial frequency is applied and the time of flight is measured as a function of the applied

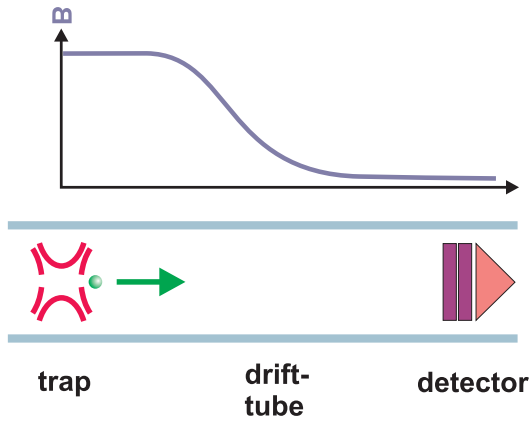

Fig. 20. Principle of the time-of-flight resonance detection technique.

frequency. Stepping through a frequency range that includes ν_c a resonance curve is obtained. In the case of a full conversion of magnetron into cyclotron motion in resonance, the curve has a minimum at $\nu_{rf} = \nu_c$. Figure 21 shows an experimental resonance curve for ^{63}Ga. The shape of the resonance curves reflects the profiles shown in Fig. 19. It is somewhat modified due to the non-linear conversion of gained cyclotron energy into a change of the time of flight.

The change in time of flight for a give radial energy E_r can be calculated if the magnetic field $B(z)$, the electric potential $U(z)$ along the ion's flight path and its initial total energy E_0 are known.

$$T(\omega_{rf}) = \int_{z_0}^{z_1} \left[\frac{m}{E_0 - \mu(\omega_{rf})B(z) - qU(z)} \right]^{\frac{1}{2}} dz \tag{41}$$

With this equation and the theoretical profile for the radial energy given by (39) it is possible to obtain a theoretical line shape for the resonances which can be fitted to the data. Such a fit is included in Fig. 21 which shows excellent agreement.

3.6 Cooling in Penning and Paul Traps

Both for beam improvement and for precision experiments ion cooling is important. Beam cooling reduces the transverse and longitudinal emittance of ion beams and is therefore of importance for more efficient beam transport or reduced Doppler width in laser spectroscopy. Cooled ions can be trapped in a smaller volume. The ions probe less of the imperfections in the trapping fields and can be manipulated with higher precision.

There are many ways to cool ions. Examples are electron cooling, which is very successfully applied to ion storage rings, or laser cooling which allows

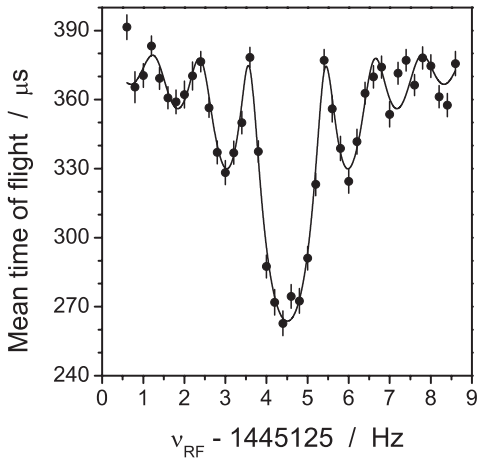

Fig. 21. Cyclotron resonance curve for ^{63}Ga measured with the ISOLTRAP experiment at CERN. Plotted is the mean time of flight of the ions to a detector after their ejection from a trap as a function of the applied rf frequency. The solid line is a fit of the theoretical line profile to the data.

temperature of $<$ mK to be achieved. The most important cooling technique in connection with radioactive beams is buffer gas cooling. Buffer gas cooling relies on collision of hot ions with a cold light buffer gas. Due to their high ionization potential noble gases are normally used for ion cooling. Buffer gas cooling is simple and fast and therefore a good choice for the cooling of short-lived rare isotopes.

The overall effect of the buffer gas on the ion motion can be seen as that of a viscous drag force $F_{fric} = -m \cdot \delta \cdot v_{ion}$, where v_{ion} is the ion velocity and δ a damping parameter describing the effect of the buffer gas. For low ion velocities δ can be assumed to be constant and to be given by the so-called ion mobility K. This quantity has been measured for many gas-ion combinations. The tabulated values of the ion mobilities K [26,27] are usually normalized to normal pressure and normal temperature. Table 3 gives a collection of mobility values for different ions in various nobel gases. Noble gases are normally used because of their high ionization potential. What is observed is that in first order the mobilities have only a small dependence on the type of ion but increase strongly with the element number of the gas.

With the ion mobility K the damping constant δ can be written as

$$\delta = \frac{e}{m}\frac{1}{K}\frac{270\,\mathrm{K}}{T}\frac{p}{1024\,\mathrm{mbar}} \tag{42}$$

Here, q is the ion's charge and T and p are the gas temperature and pressure.

The damping leads to a change of the motional amplitudes

$$\rho(t) = \rho_0 e^{-\alpha t}. \tag{43}$$

Table 3. Ion mobilities K for different ion and buffergas combinations. Values are given in units of $10^{-5}\,\frac{\mathrm{m}^2}{\mathrm{Vs}}$

	He	Ar	Kr
K^+	216(6)	27.0(8)	18.3(9)
Rb^+	200(6)	31.0(9)	14.5(4)
Cs^+	183(4)	21(1)	13.0(4)

For linear oscillatory motions like the oscillations in a Paul trap or the axial motion in a Penning trap we have $\alpha = \delta$. In the cases of the magnetron and cyclotron motion in a Penning trap the damping constants are

$$\alpha_\pm = \pm\delta\frac{\omega_\pm}{\omega_+ - \omega_-} \ . \tag{44}$$

The negative sign of α_- results in an increase of the magnetron amplitude with time, which in accordance with the total negative energy (35) of this motion. Figure 22 (left) shows the effect of a viscous damping force on the radial motion of an ion in a Penning trap. It can be seen that the amplitude of the magnetron motion slowly increases. A cyclotron motion, if present, would be damped much faster. The ratio of both damping constants is $\alpha_+/\alpha_- = -\omega_+/\omega_-$.

As an example we take cesium ions in helium in a Penning trap with parameters as given in Table 1. A helium buffer gas pressure of $p_{He} = 10^{-4}$ mbar leads to $\alpha = 34\,\mathrm{s}^{-1}$. The amplitude of the axial motion is damped with a time constant $\tau_z = 1/\alpha = 29\,\mathrm{ms}$. The time constants for the radial motions are $\tau_+ = 1/\alpha_+ = 28\,\mathrm{ms}$ and $\tau_- = 1/\alpha_- = -1.4\,\mathrm{s}$.

In order to be able to use buffer gas cooling in a Penning trap the instability of the magnetron motion has to be overcome. This can be achieved [23, 28] by coupling the magnetron motion to the modified cyclotron motion via quadrupole excitation at $\nu_c = \nu_+ + \nu_-$ as discussed above. Figure 22 (right) shows the effect of a simultaneous application of an azimuthal quadrupolar rf field at the ions cyclotron frequency. The amplitudes of both motions de-

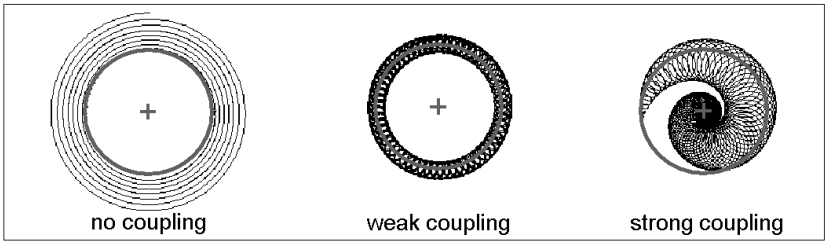

Fig. 22. Radial motion under the influence of a damping force in a Penning trap without (left) and with weak (middle) and strong (right) quadrupole excitation.

crease until the ion sits cooled in the trap center. It is important to note that this process is mass selective since the ion's cyclotron frequency is involved. In [24] it has been shown that the minimum time constant τ_{min} for this centering is determined by the buffer gas pressure and the resulting damping constant δ and is given by

$$\tau_{min} = -2/\delta \tag{45}$$

In order to reach this time constant an rf amplitude

$$V_{rf} = 2\delta B \cdot a^2 \tag{46}$$

has to be applied. Larger values for V_{rf} do not result in a faster centering.

As an example for cooling and centering in a Penning trap we assume a trap with inner diameter $\rho_0 \approx a = 2$ cm and a helium buffer gas pressure of 10^{-4} mbar. With this conditions cesium ions are centered with a time constant of $\tau_{min} = 57$ ms if an rf amplitude of $V_{rf} = 27$ mV is used.

For the macro motion in Paul traps or in other radiofrequency devices the same time constant is observed as for an axial oscillation in a Penning trap with the same frequency. An important effect of the damping to be taken into account is that it does not only influence the macro motion but also the micro motion. Due to the damping the amplitude of the micro motion will be reduced. Since this motion is the origin of the pseudo potential (see Chap. 3.2) a reduction of its amplitude will result in a reduction of the effective force F_n and a shallower potential well. If we include the effect of the damping the effective pseudo potential will have the form

$$V_{\text{pseudo}}(\rho, z) = \frac{e}{m}\left(\frac{U_r}{2d_0^2}\right)^2 \frac{1}{\omega_{rf}^2 + \delta^2}(\rho^2/4 + z^2). \tag{47}$$

For low buffer gas pressures (< 1 mbar) as used for buffer gas cooling in traps and ion guides the effect is normally negligible. The effect becomes important if much higher pressures are used as for example in gas stopping cells for fast ion beams. Some of the systems use rf fields to confine and guide the ions. If we take trap parameters as given in Table 1 as a coarse representation and a cesium ion in helium, then the depth of the potential will be reduced from 4.1 V to 0.13 V for a helium pressure of 100 mbar.

Another effect of the buffer gas is the so-called rf heating. An ion performing its fast micromotion can be "scattered" to larger macro motion orbits if it collides with a buffer gas atom. This effect limits the lowest achievable ion temperature to above that of the buffer gas. A similar effect is also observed in the case of the sideband cooling in a Penning trap discussed above as long as the azimuthal quadrupole rf-field is on. But since the rf-field can be switched off without losing the ions a post-cooling can be achieved by simply leaving the ions for some time alone in the gas and by relying on the fact that the rate of increase of the magnetron orbit is very slow.

3.7 Injection of Ions into Traps

So far we have not considered how to capture ions in traps. In the case of rare isotopes the ions are normally delivered by external ion sources. The two basic schemes for the capture of ions are a) continuous capture and b) dynamic capture. They are illustrated in Fig. 23. In the case of continuous capture the ions are slowed down to just have enough energy to overcome one side of the potential walls provided by the trapping field. In order to capture the ion a dissipative mechanism, for example the presence of a buffer gas, is required. If the energy loss is large enough the ion will finally find itself at the minimum of the trapping potential. This process allows continuous ion beams to be accumulated and automatically provides ion cooling. If desired the ions can again be released from the trap as a short ion bunch if the potential is switched as shown in the figure.

The second mechanism, illustrated in Fig. 23 requires short ion bunches. The potential is lowered at the entrance side of the trap so that an ion or ion bunch can enter the trap. When the ion is inside the trap the potential is raised again. The timing and slope of the ramp have to match the properties of the ion bunch in order to achieve minimum ion amplitudes after the capture. This capture mechanism is important if ions are to be captured under ultra high vacuum conditions as they are for example required in precision traps for mass spectrometry.

3.8 Mass Determination in Penning Traps

The basic principle of mass measurements in Penning traps is the determination of the ions' cyclotron frequency $\omega_c = e/m \cdot B$ in a known magnetic

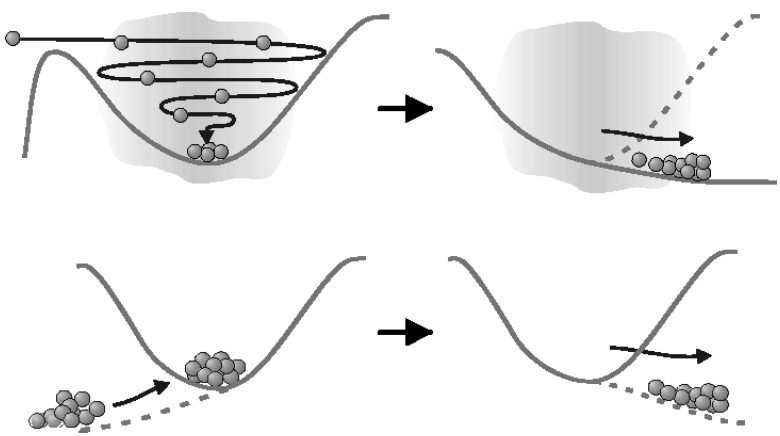

Fig. 23. Capture of ions in traps and subsequent release. Top: accumulation of continuously arriving ions in a buffer gas filled ion trap and pulsed release of cooled ions. Bottom: dynamic capture of single ions or ion bunches and subsequent pulsed release.

field B. More precisely, the quantity that can be determined is the charge to mass ratio, but normally the charge state of the ions is know or can be easily determined.

From (30) and (31) follows that the pure cyclotron frequency ω_c of an ion can either be determined by independent measurements of ν_+, ν_z, and ν_- [29] or by a direct measurement of the sum frequency $\nu_+ + \nu_-$ [23,24].

The magnetic field is usually determined by a measurement of the cyclotron frequency ν_c of a reference ion with well known mass m_{ref}^{ion}. This results in a mass ratio measurement for the ions

$$\frac{m^{ion}}{m_{ref}^{ion}} = \frac{\nu_{c,ref}}{\nu_c} \ . \tag{48}$$

Since the mass of the reference ion may be subject to change the mass ratio has to be regarded as the primary result of a Penning trap mass measurement. An exception is the case where the reference ion is ^{12}C which determines the atomic mass unit [30,31]). In this case absolute mass measurements can be made. In addition to having practically no mass uncertainty, carbon cluster ions offer the additional advantage of providing reference masses very close to each nucleus, which can minimize systematic errors.

The resolving power in Penning trap mass spectrometry depends on the time of observation T_{obs} of the ion motion. The line width $\Delta\nu_c$(FWHM) of the resonance curves as shown in Fig. 21 with which the cyclotron frequency can be determined is approximately given by $\Delta\nu_c \approx 1/T_{obs}$. For the resolving power one obtains

$$R = \frac{m}{\Delta m} = \frac{\nu_c}{\Delta\nu_c} \approx \nu_c \cdot T_{obs} \quad . \tag{49}$$

For a singly charged ion with mass number 150 in a 9-T magnetic field the cyclotron frequency is about $\nu_c = 1$ MHz. A one-second observation time gives a resolving power of 1 million. Extending the time of observation of the ion motion to ten seconds would increase the resolving power by an order of magnitude. This of course requires the nuclide to live long enough. An interesting and potentially powerful alternative is to increase the charge state and, consequently, the cyclotron frequency of the ion.

4 Application of Ion Traps to Rare Isotopes

4.1 Ideal Decay Studies

Ion clouds in traps are ideal sources for nuclear decay studies. These sources are backing free which means that scattering in the target material is avoided. Open trap designs make efficient detection of the decay products possible. The magnetic field of Penning traps can be employed to guide charged decay products to outside detectors.

Presently a couple of decay experiments in ion traps are under preparation. Most of the experiments aim at precision decay studies as required for the search for scalar and tensor currents in weak interaction [32]. One example is the WITCH spectrometer [33], which is on its way to be installed at ISOLDE. It consists of a Penning trap system for the accumulation of the ions of interest and a retardation spectrometer for a precise measurement of the ions' recoil energy spectrum. From its shape limits on scalar and tensor currents can be determined. A similar goal is followed in an experiment under development at LPC/Caen [34]. Here a "transparent" Paul trap will be used to study the decay of ^{6}He in an ion-beta correlation experiment searching for tensor currents. An new facility for studies along this line will be TRIμP at KVI/Groningen [35].

Not only for this type of precision experiments do ion traps offer advantages. For example, Penning traps can be very beneficial in the study of low-energy conversion electrons. The fundamental problem in classical spectroscopy experiments is the electron interaction with the source material. Using sources of trapped ions resolves this problem. Initial tests [36] of decay studies in Penning traps have been performed with REXTRAP [37] at ISOLDE, and look promising

4.2 Radioactive Ion Beam Manipulation

The development of new techniques for the manipulation of radioactive ion beams is actively pursued by several groups worldwide. One of the main objectives is a better matching of the properties of the radioactive ions beams to specific requirements of the experiments. Ion trap techniques have started to play an increasingly important role, in particular for the accumulation, cooling, and bunching of these beams. Both Penning traps [38] and radiofrequency multipole ion traps [39] or guides can fulfil this task. In addition, Penning traps offer high-resolution mass separation and can be used for beam purification [40].

Beam cooling, accumulation, and bunching. The basic principle of beam cooling, accumulation and bunching has already been illustrated in Fig. 23. Figure 24 illustrates a realistic scenario based on a linear radiofrequency ion trap. The trap is made of segmented quadrupole electrodes to which rf voltages are applied for the transverse confinement and dc voltages for the longitudinal confinement. In order to accumulate, cool and bunch a continuous beam, the ions are allowed to overcome the potential hill at the entrance of the trap which is filled with a light buffer gas. Passing through the potential well of the trap, the ions lose kinetic energy due to collisions with buffer gas atoms. Finally, after the ions are accumulated in the potential minimum, they can be released by lowering the potential hill at the exit side of the trap. The usefulness of this technique for beam manipulation has

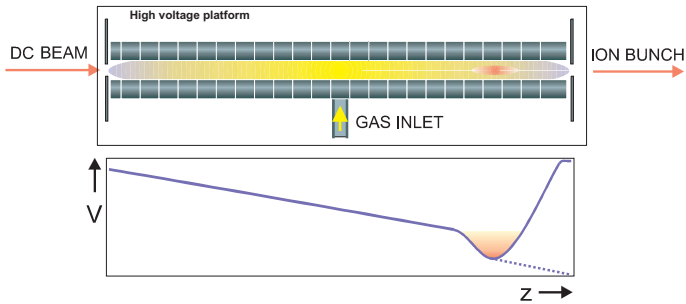

Fig. 24. Ion accumulation, cooling and bunching with a gas-filled linear radio-frequency quadrupole ion trap.

been recognized and during the last few years such systems have shown up at many radioactive beam facilities. They serve either individual experiments like ISOLTRAP [41], CPT [42] and others [43], or are installed for a general beam improvement at such facilities. A recent example is the Jyväskylä ion beam cooler and buncher [44] installed at the IGISOL on-line mass separator. This system improved the IGISOL beam emittance drastically and added the feature of bunched beams. First experiments to benefit from this were collinear laser spectroscopy studies [45,46]. Plans to install a general beam cooler exists also for ISOLDE [47].

Penning traps can also be used as ion beam bunchers and accumulators. This was first demonstrated with the cooler Penning trap of ISOLTRAP (see Fig. 26). The largest Penning-trap-based ion beam accumulator built so far is REXTRAP [37]. This system is operational and accumulates and bunches the ISOLDE ion beam for post-acceleration within the REX-ISOLDE project [48,49].

Isobar and isomer separators. Mass separation in traps can be achieved by selectively driving unwanted ions to large cyclotron amplitudes using dipole excitation at their reduced cyclotron frequency. Another possibility of mass separation is to make use of the mass selective features of the side band buffer gas cooling technique discussed above. Only those ions will be centered in the trap for which their cyclotron frequency is applied. The other ions are lost due to an increase of their magnetron motion. If desired, this process can even be accelerated by additional magnetron excitation. ISOLTRAP has demonstrated that Penning traps can be used to separate isobars in radioactive ion beams with resolving powers up to 10^5 [40] by using mass selective buffer gas cooling. New Penning trap projects that are going to employ this beam purification technique are JYFLTRAP at Jyväskylä [50] and SHIPTRAP at GSI [51,52].

An example of mass separation using a Penning trap is shown in Fig. 25 which has been obtained with the JYFL Penning trap system.

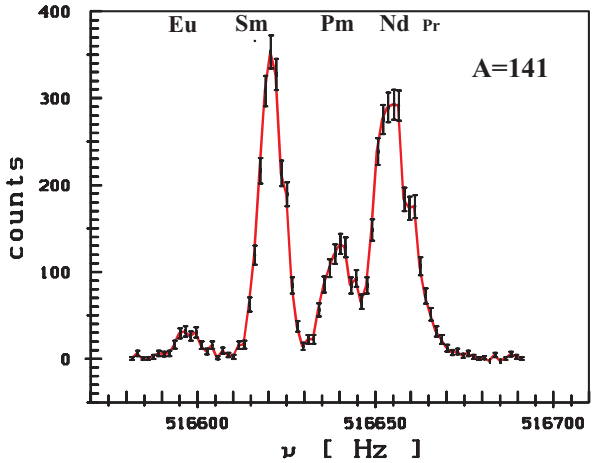

Fig. 25. Mass scan with mass selective buffergas cooling in the ISOLTRAP experiment.

ISOLTRAP has also shown that isomers can be resolved [53] even if the excitation energy is as low as 100 keV [54]. The possibility of isomer resolution in traps has recently been used also for isomer identification and isomer separation in an experiment in which decay studies, laser spectroscopy and ISOLTRAP was employed for the study of ^{70}Cu [55]. Dipole excitation at the reduced cyclotron frequency ω_+ was employed to selectively remove ions in one state from the trap.

4.3 Rare Isotope Penning Trap Mass Spectrometry (RI-PTMS)

The development of new direct mass measurement techniques have provided tools for a detailed study of nuclear binding far from the valley of stability [56–58]. Employing these tools for a systematic exploration of masses allows us to directly observe nuclear structure effects like the location of shell and subshell closures, pairing, or the onset of deformation. Masses play an important role in the understanding of nuclear astrophysical processes. However, many important nuclei in these processes are still not accessible in the lab and mass prediction by models and mass formula have to be employed [59–61]. It is clear that new and accurate mass data far from stability are the most stringent tests for the predictive power of these models. For the general exploration of nuclear structure effects an accuracy of 100 keV is often sufficient. In order to reveal more subtle effects an accuracy in the order of 10 keV may be required. There are special cases where the mass measurement accuracy must go even further. This is for example the case for testing the standard model via a precise study of super-allowed β emitters. Mass measurements with an accuracy of 1 keV or less of the parent and daughter

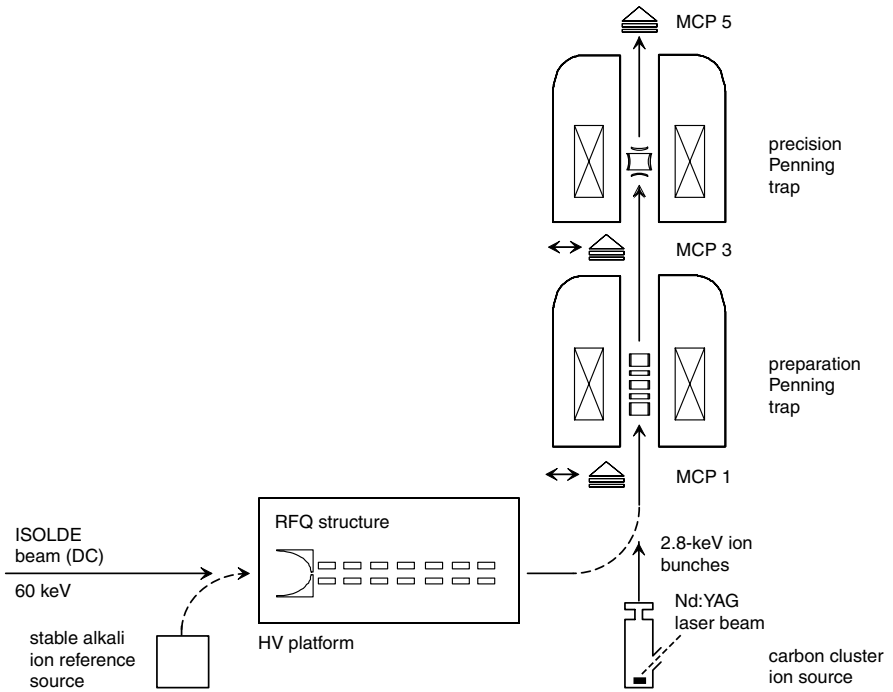

Fig. 26. ISOLTRAP mass spectrometer at ISOLDE/CERN. The main components are an RFQ trap for ion cooling and bunching, a Penning trap for isobar separation, and the Penning trap for the cyclotron frequency determination. Micro-channel plate detectors are used for the beam tuning and for the resonance detection. Two ion stable beam ion sources provide ions for the mass calibration.

nuclides of such transitions give stringent Q-values and complement nuclear spectroscopy measurements.

A variety of new techniques for the direct measurement of nuclear masses [56,57] have been developed during the past two decades. Those that are presently in use are either based on time-of-flight or frequency measurements. Frequency measurements are carried out with storage rings, transmission spectrometers, and Penning traps. The latter have proven to deliver unprecedented accuracy even for very exotic nuclides. In fact, the newest mass measurement projects for rare isotopes are all based on Penning traps. Compared to measurements on stable ions there are special requirements for Penning trap mass measurements on rare isotopes. These requirements are due to several factors: the ions are delivered by external sources, can have velocities approaching the speed of light, are often only produced in minute quantities, and have very short half-lives.

The statistical uncertainty $\delta m/m$ with which the cyclotron frequency can be determined is inversely proportional to both the resolving power R and to

Table 4. RI-PTMS on various rare nuclides (see text).

	$T_{1/2}$	T_{obs}	ν_c [MHz]	R [10^6]	N_{ion}	$\delta m/m$	δm [keV]
^{19}C	46 ms	92 ms	7.6	0.7	200	$1 \cdot 10^{-7}$	1.8
^{62}Ga	116 ms	232 ms	2.3	5.4	40000	$1 \cdot 10^{-8}$	0.5
^{131}Sn	56 s	10 s	1.1	11.0	100	$1 \cdot 10^{-8}$	1.1
^{269}Hs	9 s	2 s	0.5	1.1	100	$1 \cdot 10^{-7}$	23

the square root of the number N_{ion} of detected ions. The forefactor depends to some extent on the detection scheme on the experiment. An investigation of a large number of data obtained with ISOLTRAP showed that this factor is very close to unity resulting in

$$(\delta m/m)_{stat} \approx 1 \cdot R^{-1} \cdot N_{ion}^{-1/2} \quad . \tag{50}$$

Using the above relations the accuracy and sensitivity of RI-PTMS can be evaluated for several scenarios. This is illustrated in Table 1 for nuclides with different mass and half-life. It is assumed that the maximum storage time is twice the half-life of the investigated nuclide. The magnetic field is taken to be 9.4 T, which corresponds to the field strength available in the LEBIT project[1] at Michigan State University (MSU). Case 1 (^{19}C) illustrates a measurement on a short-lived halo nucleus. It can be seen that with only two hundred detected ions a statistical uncertainty of a few keV can be achieved, sufficient to increase understanding of the "size" of the neutron halo. Case 2 describes the situation of a high-accuracy mass measurement on a short-lived nuclide, like the super-allowed Fermi-emitter ^{62}Ga. In order to achieve a statistical accuracy as required for a meaningful test of the Conserved-Vector-Current (CVC) hypothesis several tens of thousands of ions will have to be detected. With sufficient beam intensity this can be achieved in less than a day of measurement time. Case 3 (^{131}Sn) describes the situation of a mid mass nucleus important for shell model calculations. Because of the long half-life a resolving power can be achieved, high enough to resolve the ground state and a long-lived isomeric state, and to determine its excitation energy. The last case illustrates the situation of a mass measurement of a superheavy nucleus. Of course, the total accuracy of the mass values has to include possible systematic errors. The design of present ion trap systems for nuclear mass measurements is such that systematic errors due to field imperfections are typically below $\delta m/m < 1 \cdot 10^{-8}$. Furthermore, frequent calibration measurements can ensure a similar uncertainty for the magnetic field strength determination. Some care has to be taken to avoid systematic errors due to Coulomb interaction between ions of different mass stored simultaneously [62]. Such effects can be avoided if the measurements are performed with only a single trapped ion at a time.

[1] It should be noted that all other projects discussed in this paper use magnetic fields of 6-7 T

The ability to resolve nuclear isomeric and ground states is an important feature of RI-PTMS in particular for ensuring an accurate determination of ground state masses. Nearly one third of the known nuclides have long-lived isomeric states with (in many cases unknown) excitation energies. Only in a few cases does information about the production ratio exist which may vary drastically depending on the spins, the half-lives and on the parameters of rare nuclide production. Therefore, the resolution of nuclides in their ground or isomeric state is essential for an unambiguous determination of the mass of the nuclide in either state (see for example [62,64]).

4.4 PTMS Projects at Rare Isotope Beam Facilities

ISOLTRAP. ISOLTRAP [63] at ISOLDE/CERN was the first system to demonstrate that Penning traps can be applied with advantage also to short-lived radioactive ions. The success of this experiment has triggered many more ion trap projects already installed or to be installed at rare isotope facilities. The ISOLTRAP spectrometer consists of three ion trap sub-systems. The first ion trap has the task of stopping the 60 keV ISOLDE beam and to prepare it for efficient transfer into the cooler trap. An RFQ trap ion beam [41] is used of this purpose, which allows the capture of the continuous 60 keV ISOLDE beam in flight. Short, cooled ion bunches are released and re-accelerated to an energy of about 1 keV by using a pulsed drift-tube technique. The second component is a buffer-gas filled Penning trap [40] which has the task of accumulating and purifying ions delivered by the RFQ-trap beam buncher. Isobar separation is achieved by using a mass selective buffer gas cooling technique [23,24,28]. The ions are then transported to a 6-Tesla precision trap [66]. This is the actual mass spectrometer where the cyclotron frequency of the captured ions is determined. The accuracy limit of ISOLTRAP was investigated in detail and found to be below 10 ppb [31].

More than 200 masses have been investigated with ISOLTRAP (see for example [64,67–75]. Recent ISOLTRAP highlights are the determination of the masses of ^{74}Rb [76], which has a half-life of only 65 ms and of ^{34}Ar, for which an accuracy of 400 eV was achieved [77,78]. Both cases are of importance in connection with tests of the CVC hypothesis.

JYFLTRAP in Jyväskylä. For several years the IGISOL technique [17] at the cyclotron laboratory in Jyväskylä has been providing low-energy ion beams for a rich physics program. A recent step to further improve the beam quality of the IGISOL beams was the installation of an ion beam cooler and buncher similar to the system used at ISOLTRAP. This beam buncher system is operational and has recently been used in connection with laser spectroscopy studies [45]. A second important step in the JYFLTRAP project will be the installation of a tandem Penning trap system. This trap is planned to be used as an isobar separator, which will provide clean pulsed beams for

the benefit of many experiments. The second Penning trap, which will be placed in a common 7 T magnet system, is planned to be used for precision mass measurements. The construction of the Penning trap is completed and its ability to act as an isobar separator has recently been demonstrated.

TITAN at TRIUMF/Vancouver. TITAN at the ISAC facility at TRIUMF in Vancouver is the youngest project [79]. Its unique feature will be the coupling of an electron beam ion trap (EBIT) for charge breeding to a Penning trap mass spectrometer. The gain in cyclotron frequency will boost accuracy and increase the sensitivity. Given ISAC's very high production rates, the project has the potential to extend high-accuracy mass measurements to very short-lived nuclides far off stability.

CPT at ANL. The Canadian Penning Trap CPT [42,80,81] is an ion trap project that includes stopping of energetic radioactive products from nuclear reactions in a gas cell after in-flight separation. Stable beam with an energy up to several tens of MeV/u from the ATLAS accelerator at Argonne National Laboratory is sent to appropriate targets placed at the entrance of an Enge split-pole magnet. Mass separated reaction products are retarded and stopped in a high-pressure (100-200 mbar He) gas cell. Singly or doubly charged ions are extracted out of this cell by combined static and radiofrequency electric fields. Similar gas-stopping ion guiding scheme is also used at SHIPTRAP and LEBIT (see below) and at RIKEN [82]. They are guided into a high vacuum region by employing multi-stage differential pumping and radiofrequency quadrupole systems which act as an ion guide, accumulator and buncher. The ion bunches are then trapped in a Paul trap for further cooling and finally captured in a Penning trap (B=6T) where the mass measurement takes place. First results from CPT include measurements on neutron-deficient cesium isotopes [80] and on ^{68}Se [83]. Furthermore, measurements were made on fission fragments produced by a fission source placed in front of the gas cell window.

SHIPTRAP at GSI and MAFFTRAP at LMU. SHIPTRAP [51] is presently under construction and testing at GSI/Darmstadt and is installed at the velocity filter SHIP. The goal of the project is to set up a facility for the precise study of properties of transactinides and superheavies. In addition to mass measurements this may include at a later stage decay studies, laser spectroscopy and ion chemistry studies. The SHIP reaction products (typical energy several MeV/u) will be converted into a low-energy high-quality pulsed beam using a concept very similar to the one applied in the CPT project at Argonne. The separated reaction products will be stopped in a gas cell [84] and also here RFQ ion guides will be used to guide, cool and bunch the beam. The ions will finally be sent into a tandem Penning trap mass spectrometer where the first trap will be used for mass selective buffer gas cooling, and

the second for the actual mass measurement. Both traps are placed in a single ($B = 7\,\mathrm{T}$) superconducting magnet system similar to JYFLTRAP. First stopping tests have been performed, and stable ions have been trapped.

A system very similar to SHIPTRAP is foreseen to be incorporated into the planned MAFF facility (Munich Accelerator for Fission Fragments) at the new research reactor FRM-II in Munich. MAFF will produce high-intensity neutron-rich radioactive isotopes with energies up to about 6 MeV/u. The experimental activities planned at MAFFTRAP [85] will focus on nuclear spectroscopy studies and nuclear mass measurements, including superheavy nuclei produced in fusion reactions.

PTMS with high-energy rare isotope beams - LEBIT at MSU. The only Penning trap project presently under construction for mass measurements on rare nuclides produced at energies above 100 MeV/u is LEBIT [86] at NSCL/MSU. The recently upgraded coupled-cyclotron facility delivers a large range of nuclides with high intensities even very far from stability [87, 88]. Hence, it is ideally suited for a systematic exploration of nuclear binding energies of very exotic nuclei.

Figure 27 shows the layout of the LEBIT facility. As in the case of the medium-energy projects discussed above, the in-flight separated reaction products are stopped in a gas cell after passing through appropriate degraders. The particular difficulty to be overcome is the high energy and the large energy spread of the reaction products which either requires a very large gas stopping cell or a very high gas pressure. The latter option is presently pursued at the NSCL and a 1 bar gas cell of 0.5 m length is used. A combination of DC electric fields, created by a set of focusing electrodes, and gas flow through a nozzle are employed to extract ions from the gas cell. Radiofrequency quadrupole (RFQ) ion-guide techniques combined with differential pumping are used to form a low-energy ion beam. The beam is then

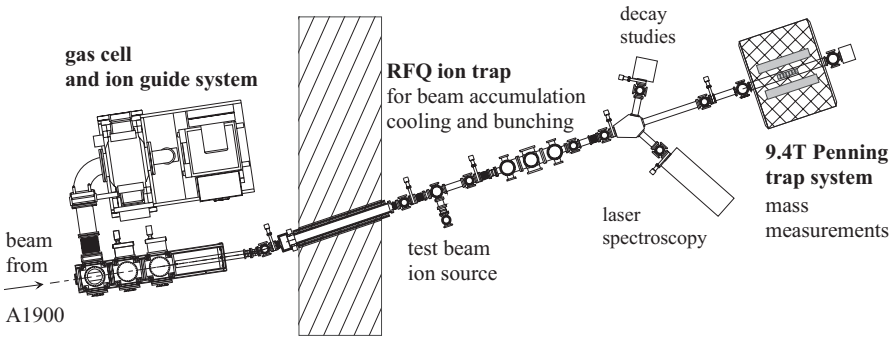

Fig. 27. General layout of the LEBIT facility. The main components are a gas stopping station for the high-energy fragmentation beams, a cryogenic RFQ trap ion cooler and buncher, and a 9.4 Tesla Penning trap mass spectrometer.

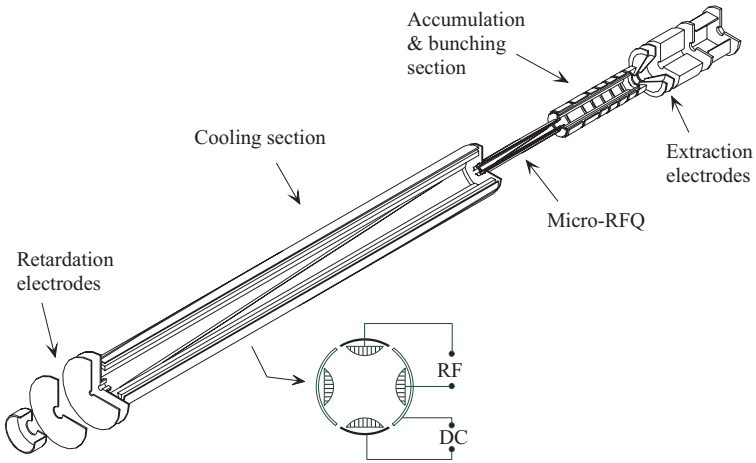

Fig. 28. Electrode system of the LEBIT ion beam buncher

transported to a cryogenic ion cooler and buncher, and subsequently to the experimental stations. The first experimental set-up will be a high-performance Penning trap mass spectrometer. The setup of the LEBIT system is nearly completed.

The ion accumulator and buncher in the LEBIT project is a linear Paul trap system designed to accept the 5 keV-DC beam from the gas cell and convert it into low-energy low-emittance pulsed beams [89]. The electrode system of the LEBIT buncher is sketched in Fig. 28. The design differs considerably from that of conventional RFQ bunchers [90,91] as used in most other projects. The two functions of the device – cooling and bunching – are performed in separate sections. A high-pressure part ($p_{He} \approx 1{\cdot}10^{-1}$ mbar) provides fast and efficient cooling whereas a low-pressure trapping region ($p_{He} \leq 1{\cdot}10^{-3}$ mbar) allows the formation of ion bunches with low energy-spread and avoids reheating of ions during ejection. A miniature RFQ couples the two sections and provides differential pumping. Novel cylindrical wedge-type electrodes allow axial guiding fields to be created without the need for segmented rods. This scheme drastically reduces the number of electrodes and decouples the application of DC and rf voltages. Another innovative feature for this buncher is its operation at LN_2-temperature. Compared to a room-temperature system the emittance of the ejected ion bunches is expected to be reduced by a factor of $T_{room} / T_{LN_2} \approx 4$. Furthermore the cold system will keep the buffer gas clean which is essential to avoid problems due to charge-exchange reactions.

A 9.4 T Penning trap system will be the first set-up in the experimental area of the LEBIT facility. Figure 29 shows a sketch of the beam-line including the Penning trap system. LEBIT uses a high performance 9.4 T magnet with 5 inch room temperature bore manufactured by Cryomagnet-

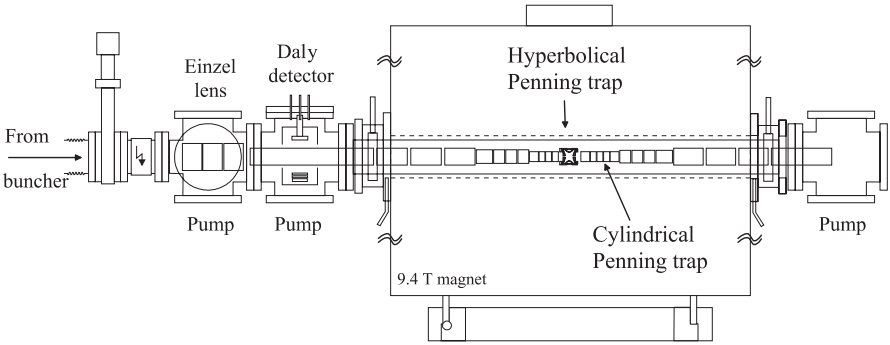

Fig. 29. Schematic layout of the LEBIT Penning trap section.

ics. The system has been installed and energized. The standard design of this actively-shielded magnet has been upgraded with an additional external-field compensation coil as invented by G. Gabrielse several years ago [92] and used for the antiproton mass measurements at CERN. Such a measure is of great advantage for high-precision measurements in an accelerator environment where the ambient field can change frequently. The LEBIT magnet system has been measured to reduce the effect of external field changes by a factor of 250.

For the mass measurements a compensated hyperbolic trap similar to that of ISOLTRAP will be used. The construction of the Penning trap electrode system with minimized magnetic field distortion and optimized electric field is another prerequisite. A trap design will be used for LEBIT that is similar to the one used for ISOLTRAP and SMILETRAP [66]. A careful re-analysis of these largely identical systems confirmed their excellent electric field properties but also showed that magnetic field distortions can still be minimized. A general-purpose cylindrical trap for ion "parking" and decay studies will follow the hyperbolic trap. Both traps will be operated at 80 K temperature. The main reason is to achieve an excellent vacuum inside the traps which is essential for achieving highest resolving powers and for avoiding charge-exchange in the case of long storage times. For the time-of-flight resonance detection scheme a concept is presently studied in which the ion detector is foreseen to be installed in the beam-line coming from the buncher. This will free access to the traps from the rear end and thus, for example, allow mass measurements to be combined with nuclear spectroscopy.

5 Conclusions

Ion traps are devices that have gained increasing importance in nuclear physics during the last few years. They have been become a routine tool for the improvement and manipulation of radioactive ion beams. Their employment as mass spectrometers for very exotic nuclides has turned out to be

very successful. They are on their way to becoming a new tool in precision decay studies. The pace at which the number of ion trap applications and projects in nuclear physics presently grows indicates that their potential has not yet been fully exploited. New developments like cryogenic beam coolers, high-field Penning trap spectrometers or the employment of highly charged ions for mass spectrometry far from stability may be considered to be the beginning of an even more powerful generation of ion trap techniques and tools for nuclear physics.

References

1. *Trapped Charged Particles and Related Fundamental Physics, Nobel Symposium at Lysekil, Sweden, August 18-26, 1994* , ed by I. Bergström, C. Carlberg, Phys. Scripta T **59** (1995)
2. *Trapped Charged Particles and Fundamental Physics, International Conference at Monterey, CA, USA, August 31 -September 4, 1998* , ed. by D.H.E. Dubin, D. Schneider (AIP Conf. Proc. (USA) 457, 1999)
3. *Trapped Charged Particles and Fundamental Interactions, International Conference at Wildbad-Kreuth, Germany, August 26 - 30, 2002*, ed. by M. Groß, D. Habs, W. Lange, U. Schramm, H. Walther, Jour. Phys. B **36(3)** and **36(5)**, (2002)
4. K. Enders et al., Phys. Rev. A **56**, 265 (1997)
5. G. Werth: Phys. Scripta T **72**, 42 (1997)
6. R.S. Van Dyck Jr. et al.: Phys. Rev. Lett. **59**, 26 (1987)
7. V.W. Hughes, T. Kinoshita: Rev. Mod. Phys. **71**, 133 (1999)
8. H. Häffner et al.: Phys. Rev. Lett. **85**, 5308 (2000)
9. R.S. Van Dyck Jr. et al.: Bull. Am. Phys. Soc. **31**, 244 (1986)
10. T. Beier et al.: Phys. Rev. Lett. **88**, 011603 (2002)
11. G. Gabrielse et al.: Phys. Rev. Lett. **82**, 3198 (1999)
12. F. DiFillipo et al.: Phys. Rev. Lett. **73**, 1481 (1994)
13. M.P. Bradley et al.: Phys. Rev. Lett. **83**, 4510 (1999)
14. C. Carlberg et al.: Phys. Rev. Lett. **83**, 4506 (1999)
15. E. Kugler: Hyperfine Interact. **129**, 23 (2002)
16. M. Dombsky et al.: Nucl. Phys. A **701**, 486c (2002)
17. H. Penttilä et al.: Nucl. Instr. Meth. B **126**, 213 (1997)
18. Kudryavtsev Y et al.: Nucl. Phys. A **701**, 465c (2002)
19. H.G. Dehmelt: Adv. At. Mol. Physics **3**, 53 (1967)
20. N. Kjaergaard, M. Drewsen: Physics of Plasmas **8**, 1371 (2001)
21. N. Kjaergaard et al.: Phys. Rev. E. **66**, 015401(R) (2002)
22. L. Schweikhard et al.: Int. J. Mass Spectrom. Ion Processes, **141**, 77 (1995)
23. G. Bollen et al.: J. Appl. Phys. **68**, 4355 (1990)
24. M. König et al.: Int. J. Mass Spec. Ion. Proc. **142**, 95 (1995)
25. G. Gräff et al.: Z. Phys. A **297**, 35 (1980)
26. H.W. Ellis et al.: Atomic Data and Nuclear Data Tables **17**, 178 (1976)
27. H.W. Ellis et al.: Atomic Data and Nuclear Data Tables **22**, 179 (1978)
28. G. Savard et al.: Phys. Lett. A **158**, 247 (1991)
29. L.S. Brown, G. Gabrielse: Rev. Mod. Phys. **58**, 233 (1986)
30. K. Blaum et al.: Euro. Phys. J. A **15**, 245 (2002)

31. A. Kellerbauer et al.: Euro. Phys. J. D **22**, 53 (2003)
32. N. Severijns, Weak Interaction Studies by Precision Experiments in Nuclear Beta Decay, Lect. Notes Phys. **651**, 339–381 (2004)
33. M. Beck et al.: Nucl. Instr. Meth. B **204**, 521 (2003)
34. E. Liénard et al.: 'Weak interaction studies using a Paul trap'. In: *Proc. Int. Conf. on Nuclear Physics at Border Lines, Lipari, Italy, March 21 - 24, 2001*, ed. by G. Fazio, G. Giardina, F.Hanappe, G. Imme, N. Rowley (World Scientific, Singapore, 2001)
35. G.P. Berg et al.: Nucl. Instr. Meth. B **204**, 532 (2003)
36. L. Weissman et al.: Hyperfine Interactions **132**, 531 (2001)
37. F. Ames et al.: 'REXTRAP, an ion buncher for REX-ISOLDE'. In: *Exotic Nuclei and Atomic Masses ENAM 98, International Conference in Bellaire, MI, USA, 1998*, ed. by B.M. Sherrill, D.J. Morrissey, C.N. Davids, (AIP Conf. Proc. **455**, 1998) pp 927-932
38. G. Bollen, Nucl. Phys. A **616**, 457c (1997)
39. R.B. Moore, G. Rouleau: J. Mod. Optics **39**, 361 (1992)
40. H. Raimbault-Hartmann et al.: Nucl. Instr. Meth. B **126**, 374 (1997)
41. F. Herfurth et al. Nucl. Instr. Meth. A **469**, 254 (2001)
42. K.S. Sharma et al.: 'Status of the Canadian Penning Trap Mass Spectrometer at the Argonne National Laboratory'. In: *Exotic Nuclei and Atomic Masses ENAM 98, International Conference in Bellaire, MI, USA, 1998*, ed. by B.M. Sherrill, D.J. Morrissey, C.N. Davids, (AIP Conf. Proc. **455**, 1998) pp 130-133
43. S. Fujitaka et al.: Nucl. Instr. Meth. B **126**, 386 (1997)
44. A. Nieminen et al.: Nucl Instr. Meth. A **469**, 244 (2001)
45. J. Billowes et al.: Nucl. Phys. A **682**, 206c (2001)
46. A. Nieminen et al.: Nucl. Instr. Meth. B **204**, 563 (2003)
47. A. Jokinen et al.: Nucl. Instr. Meth. B **204**, 86 (2003)
48. D. Habs et al.: Hyperfine Interactions **129**, 43 (2000)
49. O. Kester et al.: Nucl. Instr. Meth. B **204**, 20 (2003)
50. J. Szerypo et al.: Acta. Phys. Pol. B **32**, 985 (2001)
51. J. Dilling et al.: Hyperfine Interactions **127**, 491 (2000)
52. G. Sikler et al.: Nucl. Instr. Meth. B **204**, 482 (2003)
53. G. Bollen et al.: Phys. Rev. C **46**, R2140 (1992)
54. S. Schwarz et al.: Nucl. Phys. A **693**, 533 (2001)
55. J. Van Roosbroeck et al.: Phys. Rev. Lett. **92**, 034313 (2004)
56. G. Bollen: Nucl. Phys. A **626**, 297c (1997)
57. W. Mittig et al.: Annu. Rev. Nucl. Sci. **47**, 27 (1997)
58. D. Lunney et al.: Rev. Mod. Phys. **75**, 1021 (2003)
59. S. Goriely, M. Arnould : Astron. Astro-phys. J. **312**, 327 (1996)
60. K.L. Kratz et al.: Ap. J. **403**, 2161 (1993)
61. B. Pfeiffer et al.: Nucl. Phys. A **693**, 282 (2001)
62. G. Bollen et al.: Phys. Rev. C **46**, R2140 (1992)
63. G. Bollen et al.: Nucl. Instr. Meth. A **368** 675 (1996)
64. S. Schwarz et al.: Nucl. Phys. A **693**, 533 (2001)
65. H. Schnatz et al.: Nucl. Instr. Meth. A **251**, 17 (1986)
66. S. Becker et al.: Int. J. Mass Spectrom. Ion Proc. **99**, 53 (1990)
67. H. Stolzenberg H et al.: Phys. Rev. Lett. **65**, 3104 (1990)
68. G. Bollen et al.: Jour. Mod. Opt. **39**, 257 (1992)
69. T. Otto et al.: Nucl. Phys. A **567**, 281 (1994)

70. D. Beck et al.: Nucl. Phys. A **626**, 343c (1997)
71. F. Ames et al.: Nucl. Phys. A **651**, 3 (1999)
72. D. Beck et al.: Eur. Phys. J. A **8**, 307 (2000)
73. J. Dilling et al.: Nucl. Phys. A **701**, 520 (2002)
74. F. Herfurth et al.: Phys. Rev. Lett. **87**, 142501 (2001)
75. K. Blaum et al.: Phys. Rev. Lett. **91**, 260801 (2003)
76. A. Kellerbauer et al: Phys.Rev. Lett., submitted (2004)
77. F. Herfurth et al.: Europ. Phys. Jour. **15**, 17 (2001)
78. F. Herfurth et al.: J. Phys. B **36**, 931 (2003)
79. J. Dilling et al.: Nucl. Instr. Meth. B **204**, 492 (2003)
80. G. Savard et al.: Hyperfine Interactions **132**, 223 (2001)
81. J. Clark et al.: Nucl. Instr. Meth. B **204**, 487 (2003)
82. M. Wada et al.: Nucl. Instr. Meth. B **204**, 570 (2003)
83. J. A. Clark et al.: Phys. Rev. Lett. **92**, 192501 (2004)
84. O. Engels et al.: Hyperfine Interactions **132**, 505 (2000)
85. J. Szerypo et al: Nucl. Instr. Meth. B **204**, 512 (2003)
86. S. Schwarz et al.: Nucl. Instr. Meth. B **204**, 507 (2003)
87. D. Morrissey et al.: Europ. Phys. Jour. **15**, 105 (2001)
88. D.J. Morrissey, B.M. Sherrill, In-Flight Separation of Projectile Fragments, Lect. Notes Phys. **651**, 113–135 (2004)
89. S. Schwarz et al., Nucl. Instr. Meth. B **204**, 474 (2003)
90. J. Äystö et al.: J. Phys. B **36**, 573 (2003)
91. F. Herfurth: Nucl. Instr. Meth. B **204**, 587 (2003)
92. G. Gabrielse, J. Tan: J. Appl. Phys. **63**, 5143 (1986)